DEMOCRATIC AND POPULAR REPUBLIC OF ALGERIA

MINISTARY OF HIGHER EDUCATION AND SCIENTIFIC RESEARCH

ECOLE NATIONALE POLYTECHNIQUE

Ecole Nationale Polytechnique

Electronic Department

In partial fulfillment of the requirement for

Engineer's Degree

Study of an OFDM based simultaneous wireless information and power transfer receiver

TCHIKOU Abderrahmane

Supervised by:

Pr.DEBBAH MEROUANE at CentraleSupelec , Huawei France R&D, Paris, France.

Pr.BELOUCHRANI ADEL at ENP Algiers, algeria.

Jury members :

President:	ADNANE MOURAD	PhD	ENP
Supervisor:	BELOUCHRANI ADEL	Professor	ENP
Examiner:	SADOUN RABAH	PhD	ENP

ENP 2018

DEMOCRATIC AND POPULAR REPUBLIC OF ALGERIA

MINISTARY OF HIGHER EDUCATION AND SCIENTIFIC RESEARCH

ECOLE NATIONALE POLYTECHNIQUE

Ecole Nationale Polytechnique

Electronic Department

In partial fulfillment of the requirement for

Engineer's Degree

Study of an OFDM based simultaneous wireless information and power transfer receiver

TCHIKOU Abderrahmane

Supervised by:

Pr.DEBBAH MEROUANE à CentraleSupelec , Huawei France R&D, Paris, France.

Pr.BELOUCHRANI ADEL de l'ENP Alger

Jury members :

President:	ADNANE MOURAD	PhD	ENP
Supervisor:	BELOUCHRANI ADEL	Professor	ENP
Examiner:	SADOUN RABAH	PhD	ENP

ENP 2018

ملخص

إن أداء الاتصالات اللاسلكية مقيَّد بشكل أساسي بسبب عمر البطارية المحدود للأجهزة اللاسلكية ، والتي غالباً ما تتعطل عملياتها بسبب الحاجة إلى استبدال / إعادة شحن البطارية يدوياً. يوفر التقدم الأخير في تقنية نقل الطاقة اللاسلكية الممكّنة للترددات اللاسلكية حلاً جذاباً يسمى الاتصال اللاسلكي اللاسلكي ، حيث تقوم أجهزة الإرسال اللاسلكية المخصصة بتوفير طاقة متواصلة ومستقرة للميكروويف عبر طاقة الهواء للأجهزة اللاسلكية. كما أن الجمع بين الطاقة اللاسلكية ونقل المعلومات يثير العديد من المشاكل البحثية الجديدة ومسائل التنفيذ التي تحتاج إلى المعالجة. الهدف من هذه الرسالة هو تصميم وتنفيذ محاكي لنظام MIMO OFDM متعدد المستخدمين على أساس معيار LTE ، ثم يتم تجهيز المستخدمين بدائرة حصاد الطاقة. يتمثل التحدي في دراسة المقايضة بين المعلومات والطاقة تحت قيود عملية مختلفة.

الكلمات المفتاحية: MIMO، OFDM، LTE.

Résumé:

Les performances de la communication sans fil sont fondamentalement limitées par la durée de vie limitée de la batterie des appareils sans fil, dont les opérations sont fréquemment perturbées en raison du besoin de remplacement / recharge manuel de la batterie. L'avancée récente de la technologie de transfert d'énergie sans fil RF offre une solution attrayante appelée communication sans fil, où des émetteurs de puissance sans fil dédiés fournissent une énergie micro-onde continue et stable par voie aérienne aux dispositifs sans fil. La combinaison de l'énergie sans fil et de la transmission de l'information soulève également de nombreux nouveaux problèmes de recherche et de mise en œuvre qui doivent être résolus. Le but de cette thèse est de concevoir et mettre en œuvre un simulateur d'un système MIMO OFDM multi-utilisateurs basé sur la norme LTE, puis les utilisateurs seront équipés d'un circuit de récupération d'énergie. Le défi consiste à étudier le compromis entre l'information et l'énergie sous différentes contraintes pratiques.

Mots clés : MIMO, OFDM, LTE.

Abstract:

The performance of wireless communication is fundamentally constrained by the limited battery life of wireless devices, the operations of which are frequently disrupted due to the need of manual battery replacement/recharging. The recent advance in RF-enabled wireless energy transfer technology provides an attractive solution named wireless powered communication, where dedicated wireless power transmitters to provide continuous and stable microwave energy over the air power the wireless devices. The combination of wireless energy and information transmissions also raises many new research problems and implementation issues that need to be addressed. The goal of this thesis is to design and implement a simulator of a multi user MIMO OFDM system based on the LTE standard, then the users will be equipped by energy harvesting circuit. The challenge is to study the tradeoff between the information and the energy under different practical constraints.

Keywords: MIMO, OFDM, LTE.

To my family ...

Acknowledgments

I would like to thank god for giving me the moral, physical strength and help.

I would like to thank Pr. BELOUCHRANI Adel and Prof. DEBBAH Mérouane, the most inspiring and motivating person I have ever met.

I would like to thank Dr.MASO MAROC, Dr.MULLER Axel, Dr.HAMIDOUCHE Kenza

who was always available.

I would like to thank the members of the jury for their

agree to evaluate our project.

I would also like to thank all the teachers of the Ecole Nationale

Polytechnique of Algiers and the Ecole preparatory of Tlemcen.

Thank you all

Contents

List of Figures

List of tables

Chapter VI

INTRODUCTION

Introduction

Recently, there has been a lot of interest in integrating energy harvesting technologies into communication networks. Several studies have considered conventional renewable energy resources, such as solar and wind, and have investigated optimal resource allocation techniques for different objective functions and topologies. However, the intermittent and unpredictable nature of these energy sources makes energy harvesting critical for applications where quality of service (QoS) is of paramount importance, and most conventional harvesting technologies are only applicable in certain environments. An energy harvesting technology that overcomes the above limitations is wireless power transfer (WPT), where the nodes charge their batteries from electromagnetic radiation. In WPT, green energy can be harvested from either ambient signals opportunistically or a dedicated source in a fully controlled manner; in the latter case, green energy transfer can take place from more powerful nodes (e.g., base stations) that exploit conventional forms of renewable energy.

Initial efforts on WPT have focused on long distance and high-power applications. However, both the low efficiency of the transmission process and health concerns with such high-power applications prevented their further development. Therefore, most recent WPT research has focused on near-field energy transmission through inductive coupling (e.g., used for charging cell phones, medical implants, and electrical vehicles). In addition, recent advances in silicon technology have significantly reduced the energy demand of simple wireless devices. WPT is an innovative technology and attracts the interest from both academia and industry; some commercial WPT products already exist, and several experimental results for different WPT scenarios are reported in the literature. With sensors and wireless transceivers getting ever smaller and more energy-efficient, we envision that radio waves will not only become a major source of energy for operating these devices, but their information and energy transmission aspects will also be unified. Simultaneous wireless information and power transfer can result in significant gains in terms of spectral efficiency, time delay, energy consumption, and interference management by superposing information and power transfer. For example, wireless implants can be charged and

calibrated concurrently with the same signal, and wireless sensor nodes can be charged with the control signals they receive from the access point. In the era of the Internet of Things, this technologies can be of fundamental importance for energy supply to and information exchange with numerous ultra-low-power sensors, which support heterogeneous sensing applications. Also, future cellular systems with small cells, massive multiple-input multiple-output (MIMO), and millimeter-wave technologies will overcome current path loss effects; in this case, it could be integrated as an efficient way to jointly support high throughput and energy sustainability.

The goal of this project is to develop a wireless communication system based on MIMO OFDM technology, where the terminals will be able not only to do decode the information, but also to use the same RF signal for energy harvesting (simultaneous wireless information and power transfer). The report is organized as follows: The first chapter summarizes the state of the art, introduces the MIMO and OFDM technology and briefly describe the architecture of the studied receivers. Chapters 2,3,4 introduce mathematical modeling of the OFDM MIMO system, starting with channel modeling, OFDM modulation and finally the MIMO technique. Chapter 5 introduces the hardware architecture of the energy harvesting part that will be implemented in the next chapter. The last chapter explains the end to end implementation of the system step by step and simulations that will be discussed.

Chapter I
State of the art

Chapter I

State of the art

I.1 Introduction

The wireless power communication Network has three major components; information gateways, the RF energy sources and the network nodes/devices.

As shown in Fig.1 the information gateways are generally known as base stations, wireless routers and relays. The RF energy sources can be either dedicated RF energy transmitters or ambient RF sources (e.g. TV towers, Wi-Fi …). The network nodes are the user equipment that communicate with the information gateways. Typically, the information gateways and RF energy sources have continuous and fixed position and in some cases, the information gateway and RF energy source can be the same. Depending on theirs geographical position the network nodes need to be inside the harvesting zone to be able to harvest RF energy and inside the information transmission zone to decode successfully the information. A minimum of RF energy captured, which variate depending on the architecture of the nodes is required to support the operations of the networks nodes. In a scenario where the information gateway and RF energy source are in same, the centralized energy harvesting zone is smaller than the information transmission zone because generally, the operating power of the energy harvesting component is much higher than that of the information decoding component [1].

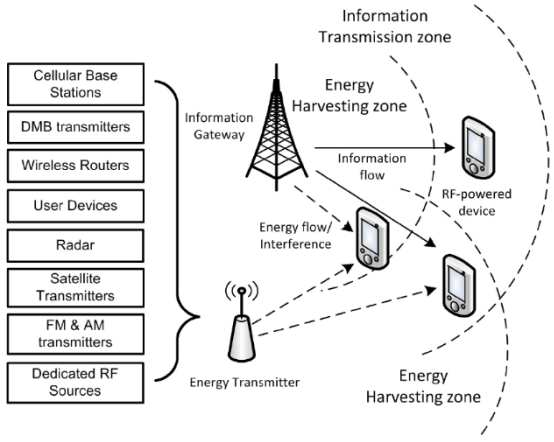

Figure 1.1 Wireless powered communication network

I.2 RF Energy propagation model

As in the wireless communication, In RF energy harvesting applications, the amount of energy that can be harvested depends on Friis free space equation parameters: the transmit power, wavelength of the RF signals, the distance between the RF energy source and the harvesting node and the polarization loss factor, which accounts for the misalignment (angle Φ) of the received electric intensity vector E and the receiver antenna linear polarization vector, this model can provide a useful upper limit for the maximum possible range available for the operating power of the energy harvesting component.

$$P_R = \cos e^2\Phi \frac{P_T G_T G_R \lambda^2}{(4\pi R)^2 L} \quad (1.2.1)$$

Where P_T and P_R are the transmitted and received power, respectively, L is the path loss factor, G_T and G_R are the transmitted and received gains, respectively, λ^2 denotes the wavelength, and $\cos e^2\Phi$ is the polarization loss factor.
The free-space model has the assumption that there is only one single path between a transmitter and a receiver without any form of environmental attenuation. However, due to RF scattering and reflection receiver may collect RF signals from a transmitter from multiple paths.
A practical and widely adopted probabilistic model is a Rayleigh model, which represents the situation when there is no line-of-sight channel between a transmitter and receiver. In the Rayleigh model:

$$P_R = P_R^{det} \times 10^L \times |r|^2 \quad (1.2.2)$$

Where P_R^{det} represents the received RF power calculated by a deterministic model, the path loss factor L is defined as $L = -\alpha \log 10(d/d_0)$, where d_0 is a reference distance, r denotes a random number following complex Gaussian distribution.

The propagation models depend on several statistical parameters which variate at each point of the information transmission and energy harvesting zones, the effects of this variation in some case could be rectified in the information decoding by adaptive algorithm but is not the case with the energy harvesting which is based on analogue circuit. To conclude; the propagation model plays a key part in the analysis and design of the RF energy harvesting model [1].

I.3 The architecture of the SWIPT receiver

This part introduces some background related to the architecture design of the SWIPT receiver, the Fig.2 shows the block diagram of a network node based on MIMO

OFDM receiver with RF energy harvesting (EH) capability to understand the practical challenges of implementing EH.

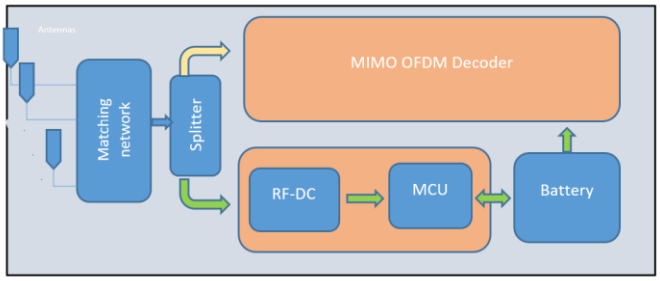

Figure 1.2 SWIPT receiver architecture

The SWIPT node consists of the following major components:

The antenna / antenna array:

An antenna is responsible for capturing RF signals, miniaturized size and high antenna gain are the main aims of antenna technology. An Antenna arrays are effective in increasing the capability for low input power. However, a tradeoff exists between antenna size and performance.

The total received power is calculated by integrating the received power P_R over frequency, therefore, a broadband antenna will receive more power than a narrowband one. As a result, wideband antennas or multi-band antennas with high gain are preferred.

The matching network:

An essential factor for any RF application is proper impedance matching to the antenna, since without a passive LC network, much of the power received at the antenna will be reflected back into free space. The specifics of this matching process vary based on the antenna, the receiving circuit input and the input power. The implementation of EH circuit which is based on nonlinear elements sensitive to the input power, increases the complexity of the matching network, therefore, the technological precision on this stage is often the most critical in the entire circuit, as even small changes in the resistive or reactive element can cause disproportionately detrimental effects.

The splitter:

Early information theoretical studies on SWIPT have assumed that the same signal can convey both energy and information without losses, revealing a fundamental trade-off between information and power transfer. However, this simultaneous transfer is not possible in practice, as the energy harvesting operation performed in the RF domain destroys the information content. To practically achieve SWIPT, the received signal has to be split in two distinct parts, one for energy harvesting and one for information decoding.

The most studied and proposed techniques in the literature to achieve this signal splitting are the Time Switching and Power Splitting[2].

The time switching (TS) switches in time between information decoding and energy harvesting. When a time switching receiver j working in the energy harvesting model, the power harvested from source i can be calculated as follows:

$$P_{j,i} = \eta P_i |h_{i,j}|^2 \quad (1.3.1)$$

Where η denotes the energy harvesting efficiency factor, P_i is the transmit power at source i, and received j and $h_{i,j}$ denotes the channel gain between source i and receiver j.
Let W and σ^2 denote the transmission bandwidth and noise power, respectively. When the time switching receiver j working in the information decoding mode, the maximum information decoding rate from source i is:

$$R_{j,i} = W\log(1 + P_i |h_{i,j}|^2 / \sigma^2) \quad (1.3.2)$$

The TS technique allows for a simple hardware implementation at the receiver but requires accurate time synchronization and information/energy scheduling.

The power splitter (PS) splits the received RF signal into two streams for the information received and RF energy harvesting with different power levels. Let $\theta_j \in [0,1]$ denote the power splitting coefficient for receiver j, i.e., θ_j is the fraction of RF signals used for energy harvesting. Similar, the power of harvested RF energy at a power splitting receiver j from source i can be calculated as follows:

$$P_{j,i} = \eta P_i |h_{i,j}|^2 \theta_j \quad (1.3.3)$$

Let σ_{SP}^2 denote the power of signal processing noise. The maximum information decoding rate at the power splitting receiver j decoded from source i is

$$R_{j,i} = W\log(1 + (1 - \theta_i) P_i |h_{i,j}|^2 / (\sigma^2 + \sigma_{SP}^2)) \quad (1.3.2)$$

Theoretically, the power splitting achieves better tradeoffs between information rate and the amount of RF energy transferred

The PS technique entails higher receiver complexity compared to TS and requires the optimization of the PS factor; however, it achieves instantaneous SWIPT, as the signal received in one time slot is used for both information decoding and power transfer. Therefore, it is more suitable for applications with critical information/energy or delay constraints and closer to the information theoretical optimum

I.4 MIMO OFDM baseband processing

A schematic representation of MIMO OFDM decoder is given in figure Fig.1.4
After digital representation of the Nr received signals is obtained by the ADCs, the decoder first must estimate and correct for the frequency offset and retrieve the symbol timing, e.g., by making use of training sequences.
After synchronization, the cyclic prefix CP is removed and the Nc-point FFT is done per branch. In the context of the unified view, at this point the Space time Frequency STF detection and decoding must be performed to recover the binary data stream. To that end, the received signals of subcarrier i are routed to the i-th MIMO detector to recover the Nt QAM symbols transmitted on that subcarrier. Next, the symbols per TX stream are

combined and, finally, STF demapping and decoding are performed on these Nt parallel streams and the resulting data are combined to obtain the binary output data.
For reliable detection, it is typically necessary that the receiver knows the wireless communication channel and keeps track of phase and amplitude drifts. To enable estimation of the wireless communication channel, the transmitter occasionally sends known training symbols [3].

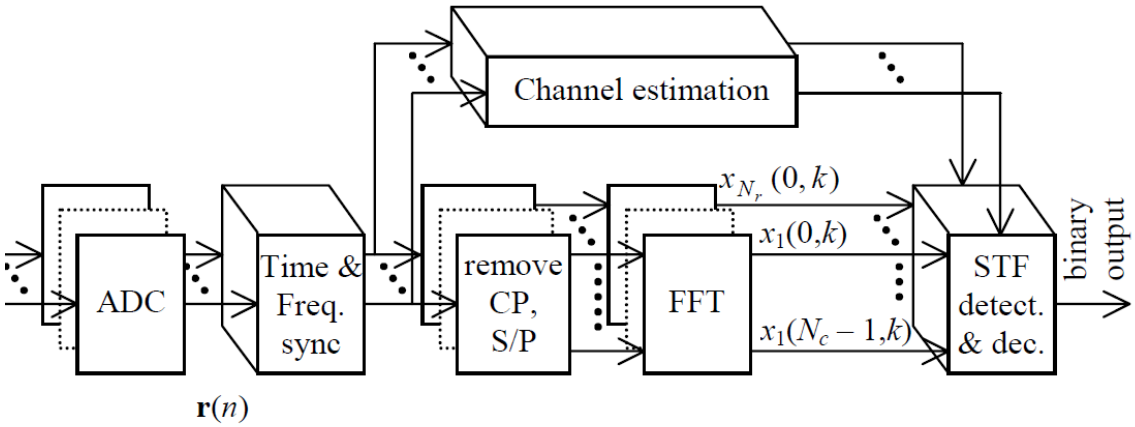

Figure 1.3 MIMO OFDM Decoder

I.5 Basic Rectifier Circuit for RF Applications

The function of a rectifier is to convert the input RF signals (AC type) captured by an antenna into DC voltage. A major challenge of the rectifier design is to generate a battery-like voltage from very low input RF power.
There are three main option for a rectifier, which are three main options for a rectifier, which are a diode, a bridge of diodes and a voltage rectifier multiplier which can be extended to n stages in cascade to achieve higher DC output voltage level.
The diode is the main component of a rectifier circuit. The rectification performance of a rectifier mainly depends the saturation current, junction capacitance and its conduction resistance of the diode(s). The most commonly used diode is silicon zero bias Schottky diode.
Power management unit (PMU) decides whether to store the electricity obtained from the RF energy harvester or to use it for information transmission immediately.
Energy storage unit or battery[5].

I.6 The tradeoff Information/Energy Harvesting

This part studies a point-to-point wireless link with simultaneous information and power transfer based on the results of The maximum achievable information rate (in bps/Hz) or the capacity of the AWGN channel is given R that can be reliably decoded at the receiver is upper-bounded by

$$R \leq \log_2(1 + hP/\sigma_A^2) \qquad (1.5.1)$$

Where h is the channel gain, P is the average transmit power and σ_A^2 is the variance of the complex Gaussian noise.

The harvested energy could be stored in the battery, denoted by Q in joule and according to the law of energy conversion, the maximum harvested energy Q to be stored in the battery cannot be larger than that received by the receiving antenna

$$Q \leq hP \tag{1.3.2}$$

Following to 1 and 2to characterize all the achievable rate (in bps/Hz for information transfer) and energy (in joules/sec for energy transfer) pairs under a given transmit power constraint P, we obtain a performance upper bound on the achievable R-E region for the system as:

$$C_{R-E}^{UB}(P) \triangleq \{(R,Q) : R \leq \log_2\left(1+\frac{hP}{\sigma_A^2}\right), Q \leq hP\} \tag{1.3.2}$$

Which is a box specified by the origin and the three vertices $(0, Q_{max})$, $(R_{max}, 0)$, (R_{max}, Q_{max}), with $Q_{max} = hP$ and $R_{max} = \log_2(1 + hP/\sigma_A^2)$. This performance bound is valid for all receiver architecture[4].

I.7 The applications of SWIPT receiver and the future market

Limited device battery life has always been a key consideration in the design of modern mobile wireless technologies. Frequent battery replacement/ recharging is often costly due to the large number of wireless devices in use, and even infeasible in many critical applications (e.g., sensors embedded in structures and implanted medical devices).

RF-enabled wireless energy transfer (WET) technology provides an attractive solution by powering wireless devices with continuous and stable energy over the air. RF-enabled WET enjoys many practical advantages, such as wide operating range, low production cost, small receiver form factor, and efficient energy multicasting.

Another performance enhancing technique for a WET is massive MIMO technology, which could significantly mitigate the effect of channel fading and enable large degree of freedom. One important application of RF-enabled WET is wireless powered communication (WPC), where wireless devices use harvested RF energy to transmit/decode information to/from other devices.

WPC is promising technology which will be an important building block of many popular commercial and industrial systems in the future, including the upcoming Internet of Things/Everything (IoT/IoE) systems consisting of billions of sensing/RFID devices as well as large-scale wireless sensor networks (WSNs) [5].

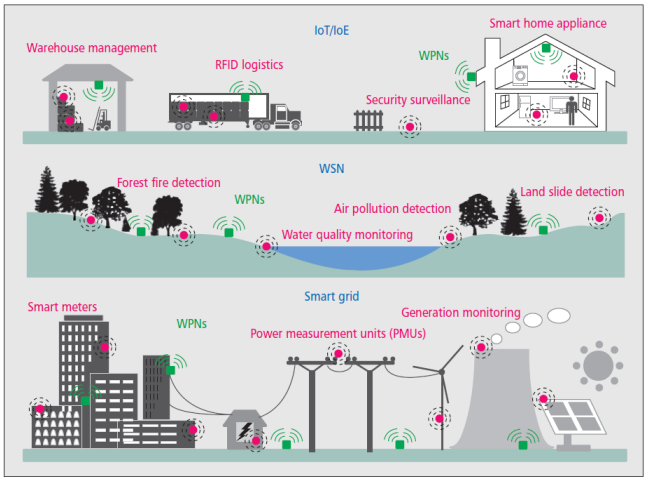

Figure 1.4 Example applications of SWIPT [5]

According to the new market research report, the wireless power transmission technology market was valued at 2.50 billion in 2016, and it is estimated to grow at a CAGR of 23.15% between 2017 and 2022 and the far-field technologies such as microwave (RF) power transmission would expect to revolutionize the market for wireless power transmission in the near future [6].

Chapitre II
Wireless Channel Modeling

Chapter II

Wireless Channel Modeling

II.1 Introduction

Wireless communications is undoubtedly the most dynamic segment in the industry of communications. As such, they have attracted the attention of the media and the imagination of the public. Cellular systems have grown exponentially over the last decade and there are currently no fewer than seven billion users in the world. Indeed, cell phones have become an essential a part of everyday life in most countries of the world. In addition, because of their flexibility and mobility, Wireless Local Area Networks (WLANs) tend to replace wired networks in homes, businesses, and campuses. Many new applications, including wireless sensors, highways, automated plants, and smart homes, have emerged, which indicates a radiant future for wireless. Or the performance of communications systems are mainly governed by the mobile radio channel, which is the subject of this chapter.

II.2 Historical

The initial understanding of the propagation of radio waves goes back to James Clerk Maxwell work, who in 1864 formulated the theory of electromagnetic propagation which predicts the existence of radio waves. In 1887, the physical existence of these waves demonstrated by Heinrich Hertz. The work of Maxwell and Hertz has launched the field. In 1894 Oliver Lodge used these principles to build the first communication system but its transmission distance was limited to 150 meters. Very quickly, the possibilities offered by the triode, a cathode lamp capable to amplify an electrical signal, invented by Lee de Forest in 1906. In the same year, Fessenden, a Canadian inventor, had worked with General Electric to build alternators delivering current of a frequency of 100 kHz and of which it is able to modulate the amplitude by the low frequency signal of the human voice. He made the first radio program for boats in the North Atlantic [7].

II.3 Mechanisms of propagation

In wireless communication, radio propagation refers to the behavior of wave's radio when they are propagated from the transmitter to the receiver, and these are three physical phenomena, namely [8]:

- Reflection: It is the physical phenomenon that occurs when an electromagnetic wave encounters an object with very large dimensions relative to the length of wave, for

example, the surface of the earth and buildings. Part or all of the electromagnetic wave is moving towards its origin.

- Diffraction: When the connection between the transmitter and the receiver is obstructed by a surface with sharp irregularities such as peaks, hills and buildings, there is diffraction that is to say that the radio waves undergo a deviation. The deviation is greater near the obstacle and decreases with the distance from it.

- Scattering: is the dispersion of electromagnetic waves when they encounter obstacles whose dimensions are small with respect to wavelength, such as road signs, trees, vehicles as well as streetlights.

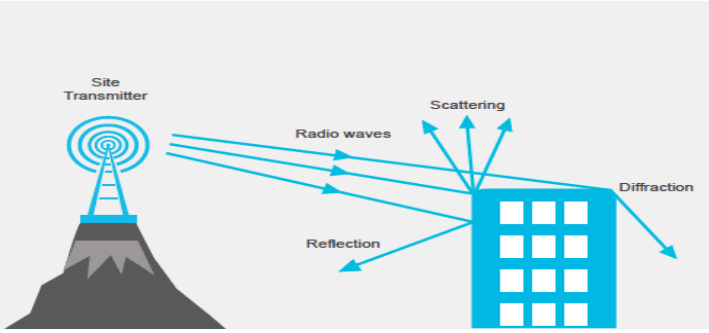

Figure 2.1 Phenomenon of propagation

II.4 Multi-path propagation

In most environments, generally the receiver is not in line of sight of the transmitter, that is to say that the receiver is in the NLOS situation. All the radio waves received arrive by different paths coming from the interaction of the signal emitted with the many obstacles present in the environment by physical phenomena cited above, namely reflection, diffraction, and scattering. These electromagnetic interactions are not without effect on the waves that undergo them. Indeed, in addition to mitigating their power, these interactions modify the parameters of the wave like its polarization and its phase. Therefore the received signal is the sum of several replicas of the transmitted signal with different amplitudes, phases and arrival times [9].

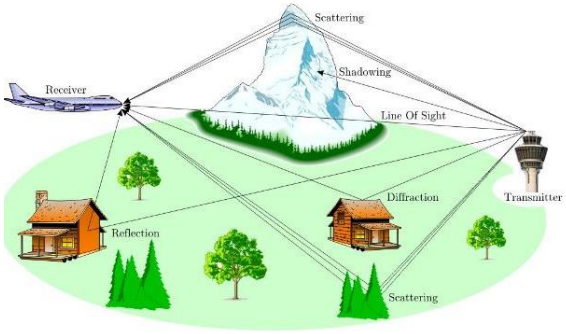

Figure 2.2 Multi-path propagation [10]

II.5 The noise

Noise gathers all the signals that do not carry useful information and come disturb the desired signal. This is a perturbation whose origins are the propagation channel (external noise) and the electronic devices used in the receiver (internal noise).

External noises may be of extraterrestrial or terrestrial origin. The first category taking into account that in the space links or in the uplinks to satellites, only the terrestrial noise sources remain. They regroup the noise caused by the atmospheric parasites, those from various environmental radiation, interference between users of the propagation channel or industrial noise and due to human activity in general. As for the internal noise, it is caused by the random movement of the electrons (they generate currents and parasitic voltages to the useful signal) present in the electronic components of the receiver [11].

II.6 Time-varying of the channel

The temporal variability of the propagation channel is an important element in understanding of the propagation of the waves. Indeed, this is the image of the movements of the different elements of the medium considered: movement of the transmitter and / or receiver, pedestrians, vehicles, etc. These temporal variations induce a frequency of offset between the frequency of the wave emitted and that of the received wave. This phenomenon is better known under the name Doppler Effect and will be further developed [12].

II.7 Models of propagation channels

The design of an effective communication system depends on the accuracy of the representation of the actual channel. There are two main approaches to modeling a propagation channel [13]

The deterministic approach: The propagation channel is modeled by a set of rays whose paths at the receiver are characterized according to the laws of diffraction, reflection and transmission phenomena based on the Fresnel laws. The advantage of these models is that they offer a complete description of the received waves. On the other hand, they require precise knowledge of the propagation environment as the dielectric properties of the environment through which the signal propagates, should be emphasized that modeling of the canal with deterministic methods remains incomplete because they do not take into account the time-varying of the channel, thus the deterministic approach is not preferred.

The statistical approach: The statistical models aim to describe the evolution of the parameters of the channel by the statistical laws in order to obtain the most realistic representation possible.

II.8 Representation of the propagation channel

II.8.1 Mathematical Formulation

The channel which varies randomly in time (dynamic channel) corresponds to a time-varying linear filter and impulse response $\mathrm{h}(\mathrm{t},\tau)$ which is expressed in the following way:

$$\mathrm{h}(\mathrm{t},\tau) = \sum_{n=1}^{N(t)} a_n(t)\delta(\tau - \tau_n(\mathrm{t}))e^{-j\varphi_n(t)} \qquad (2.1)$$

Where

$N(t)$: the number of paths on the channel.
$a_n(t)$: the attenuation factor of the nth path.
$\tau_n(\mathrm{t})$: the propagation delay of the nth path.
$\varphi_n(t)$: the phase of the n^{th} path.

The received signal $r(t)$is then connected to the transmitted signal $s(t)$ by the following relation:

$$\mathrm{r}(\mathrm{t}) = s(t) * h(\mathrm{t},\tau) + n(t) = \int_{-\infty}^{+\infty} h(\mathrm{t},\tau)\mathrm{s}(\mathrm{t}-\tau)\mathrm{d}\tau + \mathrm{n}(\mathrm{t}) \qquad (2.2)$$

Where

$\mathrm{n}(\mathrm{t})$: the complex Gaussian white noise.
$*$: represents the linear convolution product.

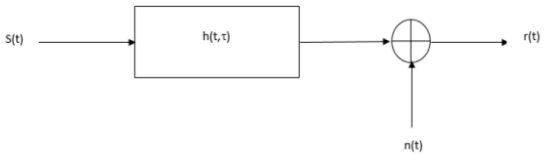

Figure 2.3 Mobile radio channel model

We can then define the frequency response of the channel which is none other than the Fourier transform of the impulse response:

$$\mathrm{H}(\mathrm{t},\mathrm{f}) = \int_{-\infty}^{+\infty} h(t,\tau)e^{-j2\pi f\tau}\,d\tau = \sum_{n=1}^{N(t)} a_n(t)e^{-j(2\pi f\tau_n(t)+\varphi_n(t))} \qquad (2.3)$$

From this expression it can be seen that the frequency response is not flat which may cause a deformation of the signal transmitted at reception.

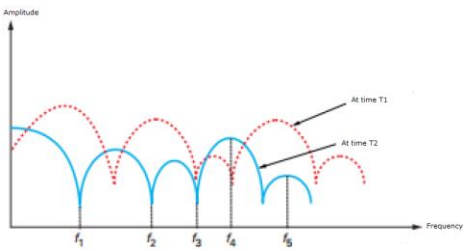

Figure 2.4 Example of transfer function of a multi-path channel [14]

II.8.2 Hypotheses

The modeling of the propagation channel according to Bello can only be applied the hypothesis of the WSSUS channel, and this hypothesis imposes two conditions [15]:

- The impulse response is stationary in the broad sense:

It is easy to see that the impulse response of the channel is a random process. In order to simplify the study of this random process, Bello makes the hypothesis known as stationarity in the broad sense. A random process is said to be stationary in the broad sense if its autocorrelation function is independent of the origin of time.

To illustrate this hypothesis, we consider the impulse response defined previously, its autocorrelation function is then written:

$$R(t_1, t_2, \tau_1, \tau_2) = E[h(t_1, \tau_1)h^*(t_2, \tau_2)] \quad (24)$$

Stationarity in the broad sense:

$$R(\Delta t, \tau_1, \tau_2) = E[h(t, \tau_1)h^*(t + \Delta t, \tau_2)] \quad (2.5)$$

Where

$\Delta t = t_1 - t_2$.

$[]^*$: represents the conjugated complex operator.

$E[]$: represents the operator expectation mathematics.

This condition means that the correlation between the power of a path at time t_1 and at time t_2 depends only on Δt.

- uncorrelated diffusers:

This condition assumes that the echoes received by the receiver originate from uncorrelated sources, it assumes that two echoes with different delay times are uncorrelated. Mathematically this results is:

$$R(\Delta t, \tau_1, \tau_2) = 0 \; \forall \; \tau_1 \neq \tau_2 \quad (2.6)$$

Thus the WSUS hypothesis implies that the autocorrelation function no longer depends on four time variables but two, as follows:

$$R(\Delta t, \tau) = E[h(t, \tau)h^*(t + \Delta t, \tau)] \quad (2.7)$$

II.8.3 Power profile of delays and characteristic parameters

II.8.4 Power delay profile

In order to characterize the power of the different paths according to their delays, the notion of power profile of delays or PDP is introduced. The PDP is defined by

$$PDP(\tau) = |h(\tau)|^2 = \sum_{n=0}^{N} |a_n|^2 \delta(\tau - \tau_n) \quad (2.7)$$

Generally, the propagation profile is modeled by a decreasing exponential since each delayed pulse usually has less power than the previous one.

II.8.5 Characteristic parameters

- The temporal dispersion:

The delay spread denoted σ_{max} is a type of distortion that occurs in a multi-path channel, that is, the received signal is the sum of several replicas of the signal transmitted with d (delays) and it corresponds to the difference in time between the arrival times of the first multipath component and the last one. The temporal dispersion and the RMS9 value of the temporal dispersion are given by the following relationships [16]:

$$\sigma_{max} = \tau_N - \tau_1 \quad (2.8)$$

$$\sigma_\tau = \sqrt{\frac{\sum_{n=0}^{N} |a_n|^2 (\tau - \tau_n)^2}{\sum_{n=0}^{N} |a_n|^2}} \quad (2.10)$$

τ^* : is the average time dispersion defined by:

$$\tau^* = \sqrt{\frac{\sum_{n=0}^{N} |a_n|^2 \tau_n}{\sum_{n=0}^{N} |a_n|^2}} \quad (2.11)$$

The Typical values of σ_τ in an outdoor environment for a 4th generation system, are approximately microsecond, and 10 to 50 nanoseconds in an indoor environment.

- Coherence band:
  The coherence band denoted B_C is a statistical measure of the frequency band over which the channel can be considered flat. It is defined approximately by the following relation [17]

$$B_C \approx \frac{1}{2\sigma_\tau} \quad (2.13)$$

  It is important to note that the relationship between temporal dispersion and the coherence band does not exist and that the previous equation is approximate.
- Doppler Band:
  The Doppler Effect is due to the movement of the receiver and / or the transmitter. When considering a single-path propagation with fc the transmitted frequency, the frequency received fr will then be $f_r = f_c + f_D$, where f_D is the Doppler shift which is given by the following relation:

$$f_D = \frac{v f_c}{c} cos\alpha \quad (2.14)$$

Where:

f_c : the carrier frequency.

v : the speed of the mobile.

α : Doppler angle between the axis of the beam and the axis of displacement of the receiver.

c : the speed of light.

The maximum Doppler frequency is obtained for $\alpha = 0$, that is to say when the mobile receiver moving towards the transmitter.

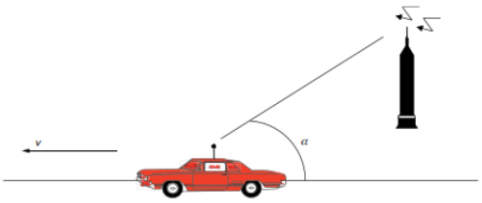

Figure 2.5 Moving vehicle and Doppler shift [18]

However, the channel is not a single path but multi-paths. Thus, for a transmitted frequency, several Doppler shift frequencies are received according to the different angles of arrival α_n of the n paths considered. Each Doppler frequency f_{D_n} associated with the same path is calculated by:

$$f_{D_n} = \frac{v f_c}{c} cos\alpha_n \quad (2.15)$$

In addition, when transmitting over a frequency band, several Doppler shift frequencies are received for each of the transmitted frequencies. A Doppler frequency band is thus received, the width B_D of which is equal to twice the maximum Doppler frequency.

- The coherence time :

  The coherence time T_C is the equivalent in the time domain of the Doppler band. It characterizes the variant nature in time of the channel. The Doppler dispersion and the coherence time are inversely proportional and subsequently approximated by[19]:

$$T_c \approx \frac{1}{B_D} \quad (2.16)$$

II.8.6 Impacts on digital communication

A thorough characterization of the propagation channel makes it possible to improve the quality of a digital transmission system. Thus, it is interesting to present the link

between the characteristic parameters of the channel and the information transmitted. This information can be represented by two parameters [20]:

- The symbol time T_c , which corresponds to the duration of a symbol.
- The band B_S , which is the spectral occupancy of the transmitted information.

II.8.7 Time fading

- Fast fading:

If $T_S \gg T_c$, then the channel is said fast fading. With this condition, the channel impulse response varies significantly over the duration of a symbol. The channel is then selective in time.

- Slow fading:

If $T_S \ll T_c$, then the channel is said slow fading. With this condition, the impulse response of the channel does not vary over the duration of a symbol. The channel is then non-selective in time.

II.8.8 Frequency fading

- Frequency selective channel:

If $B_S \gg B_c$, then the channel is said to be selective in frequency. In this case the spectrum of the received signal will be deformed outside the coherence band. The frequency selectivity condition can be reformulated in the time domain as follows:

$$\sigma_\tau \gg T_s$$

The foregoing relationship means that the frequency selectivity corresponds to inter-symbol interference or ISI interference generation in the time domain, which leads to a degradation of the performance of a digital transmission system.

- Flat fading channel:

In the event that $B_S \gg B_c$ $(\sigma_\tau \gg T_s)$ all the frequencies of the spectrum of the emitted signal undergo the same amplifications or attenuations. Consequently, the channel is considered as non-selective (no ISI in the temoprel domain) in frequency and therefore in flat fading.

II.8.9 Space fading

These fainting can be broken down into two categories:

II.8.9.1 Small Scale fading

The small scale fading is the consequence of the rapid fluctuations of the transmitted signal over short periods of time (in the order of the carrier period) or short distances (in the order of the carrier wavelength). It is due to constructive and destructive interference of multipath propagation and it becomes more relevant to the design of reliable and efficient communication systems.

In this section the main statistical models for small scale fading are overviewed.

- Rayleigh Fading:

The Rayleigh Fading is one of the most used models. It describes as a propagation scenario in which there are many objects in the environment between the transmitter and the receiver.
If the overall signal is composed by a large number of statistically independent reflected and scattered paths with random amplitudes and phase evenly distributed between 0 and 2π radians, then the contribution of each path in the tap gain $h_l\,[m]$ can be modeled as a circular symmetric complex random variable. Each gain $h_l\,[m]$ is a sum of large number of such small independent circular symmetric random variables and thus, thanks to the Central Limit Theorem, it can be modeled as a zero-mean Gaussian random variable with variance σ_2^2 , or $CN(0,\sigma_2^2)$for brevity. The magnitude $|h_l\,[m]|$ of the l^{th} gain is a random variable with Rayleigh distribution and pdf expressed as

$$f_X(x) = \frac{1}{\sigma_2^2} e^{-\frac{x}{\sigma_2^2}}, x \geq 0. \tag{2.19}$$

- Rician Fading:

When we still have large scattered paths but the LoS component becomes not negligible, we can no longer refer to Rayleigh Fading. In this case, hl [m] can be modeled as

$$h_l\,[m] = \sqrt{\frac{K}{K+1}}\,\sigma_l e^{i\theta} + \sqrt{\frac{K}{K+1}}\psi, \tag{2.19}$$

where $\psi \sim CN(0,\sigma_2^2)$, the first term is accounts for the LoS path arriving with uniform phase θ and the second term accounts for the aggregation of scattered or reflected paths that are assumed independent of θ. The parameter K is named Rician K-factor and is defined as the ratio between the power of the direct component and the power of the scattered components. In particular, when K is large (say 4-6 dB), the channel may be considered as deterministic; instead when K = 0, it reduces to the Rayleigh Fading one. Under these conditions the magnitude of $h_l\,[m]$ is Rician distributed.

- Nakagami Fading

Some experimental data does not fit into either of the distributions previously described. There exists an alternative fading distribution whose parameters can be adjusted to fit a variety of empirical measurements. This distribution is called Nakagami Fading and it is given by

$$f_X(x) = \frac{2m^m x^{2m-1}}{\Gamma(m)P_r^m} exp\left\{-\frac{mx^2}{P_r}\right\}, m \geq 0.5, \tag{2.20}$$

where P_r is the average received power and $\Gamma(.)$is the Gamma function.
However, in this work Nakagami Fading is never used; for this reason it is not dealt with in details.

II.8.9.2 Large Scale Fading

Large scale fading is the result of signal attenuation due to signal path loss over large distances and shadowing around large objects in the propagation path. It is more relevant to issues such as cell-site planning.
In this section path loss and shadowing phenomena will be treated.

- Path Loss

The reduction of an electromagnetic wave, propagating in LoS condition, in terms of power density is named **F**ree **S**pace **P**ath **L**oss (FSPL). We can estimate this power loss, as a function of the distance between the transmitter and the receiver d, using the Friis's formula

$$\frac{P_r}{P_t} = G_t G_r \left(\frac{\lambda_c}{4\pi d}\right)^2 \tag{2.21}$$

where P_r and P_t are the received and the transmitted power respectively, G_r and G_t are the gains of the receive and transmit antennas respectively and λ_c is the carrier wavelength.
For isotropic transmitting and receiving antennas (G_r = G_t= 1 = 0 dB) the Free Space Path Loss is defined as

$$L_f = \frac{P_t}{P_r} = \left(\frac{\lambda_c}{4\pi d}\right)^2 \tag{2.22}$$

However, most of the times we can not assume a pure LOS wave propagation and for this reason the signal in land mobile application do not experience free space propagation. A more appropriate theoretical and empirical models are needed.
Ray-Tracing is a well known channel characterization in which the solution of Maxwell's equations are approximated and a finite number of reflectors are assumed. We list here the main models: Two-Ray Model, 10 Ray Model and the General Ray Tracing Model among the analytical models and the Okumura Model, Hata Model and COST 231 among the empirical models.

II.8.10 Shadowing

Shadowing is caused by obstacles between the transmitter and receiver that attenuate signal power through absorption, path loss, diffraction, and fading.
Whenever an electromagnetic wave carrying the information signal, hits a surface, a part of its energy is absorbed by the surface and the other continues until it reaches the receiving antenna. This phenomenon is called reflection. Based on the scenario (rural or urban), thus, the transmitted signal can be reflected several times by obstacles (buildings, hills, etc.) before it reaches at the receiver.
When the electromagnetic wave trajectory is deviated by an obstacle we talk about the diffraction phenomenon. Another type of reflection is named scattering; it can occur in the atmosphere or in reflections from rough surfaces. In this case the signal energy is spread in all directions producing a very large number of individual paths. Due to such phenomena the received signal can be composed by a LoS component and a combinations reflected, scattered and diffracted copies of the original one.
Fig. 2.6 shows an example of scenario with multipath propagation; note that the LoS component is also shown. A transmitted signal will, thus, experience random variation due to obstacles it encounters during its path. It is clear that a model for the random

attenuation due to these effects is also needed. Since the randomness of blocking obstacles, localization, size etc., a statistical model may be conventionally used.
The most used model for this additional attenuation, empirically confirmed [21, 22], is the Log-Normal Shadowing. The fundamental characteristic of this model is that the ration

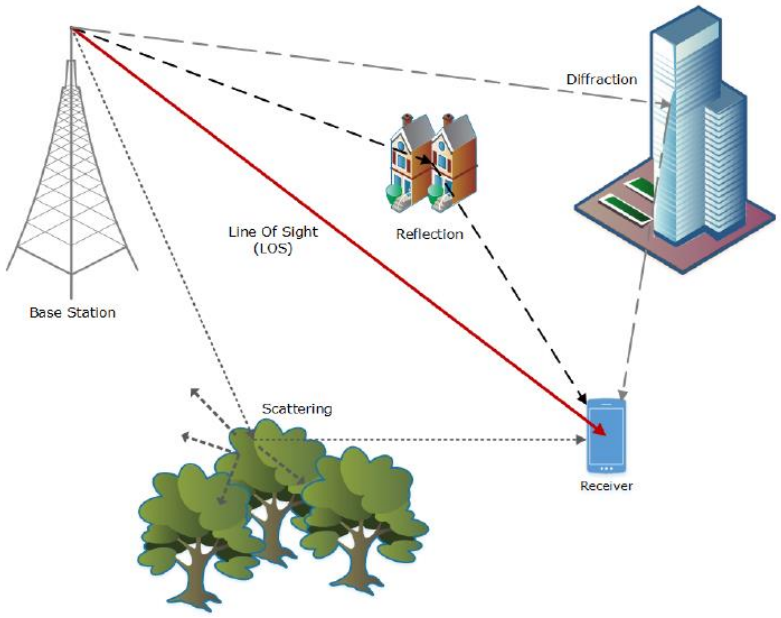

Figure 2.6 Multipath propagation scenario

between the transmitted and the received power, P_t and P_r respectively, is assumed to be a random variable log-normally distributed. Its pdf can be expressed as

$$f_X(x) = \frac{\xi}{\sqrt{2\pi}\sigma_{dB}x} \exp\left[-\frac{(10\log_{10}x - \mu_{dB})^2}{2\sigma_{dB}^2}\right], x > 0 \qquad (2.22)$$

where $x = P_t/P_r$, $\xi = 10/ln10$, $\mu_{db}$is the expected value of $x_{dB} = 10\log_{10}x$ in [dB] and $\mu_{db}$is the standard deviation of x_{dB} also in [dB].
Note that the random variable x can only takes values greater than or equal to 0 because it is physically impossible to have $x < 1, P_t < P_r$.

II.8.11 Diversity

One of the most effective techniques for mitigating the effects of fading is to use the diversity. Diversity is based on the fact that replicates of the same signal, generated by multi-path propagation, have a low probability of experiencing profound fainting simultaneously. Thus, the idea behind diversity is to combine, on reception, variants of the transmitted signal whose fluctuations are decorrelated in such a way that the fading of the resulting signal is reduced [24].

Diversity can be applied in various ways [25]:

- Temporal diversity: copies of the signal are retransmitted during various slots spaced apart by at least the coherence time of the channel.
- Frequency diversity: here the copies of the signal are transmitted on different frequencies (spaced apart by at least the coherence band of the channel).
- Polarimetric diversity: it uses the signals transmitted simultaneously by the same antennas on orthogonal polarizations that are often affected differently by the propagation medium.
- Spatial diversity: In this case the is based on multiple antennas at the emitter and / or receiver, spaced at least half the length to have a decoupling between the fades affecting the received signals by each antenna [24].

Chapter III

OFDM

Chapter III

OFDM

III.1 Introduction

OFDM stands for Orthogonal Frequency Division Multiplexing. It was described for the first time by Rober Chang in [27] in 1966 but it only after the work of Weinstein and Ebert [26] in 1971, OFDM was seen as a viable option. What put OFDM into commercial use was the Fast Fourier Transformation (FFT) usage. Before the digital implementation of OFDM via the FFT, in fact, communication systems required banks of signal generators to produce the orthogonal channels. This was basically impossible due to the high costs.

This modulation technique has been suggested for use in several contexts such as cellular radio, radio audio broadcasting, digital video broadcasting and wireless LAN systems as IEEE 802.11a, LTE, DVB.

In this chapter we first treat the principle of OFDM suited for our purposes and at the end drawbacks and advantages of such modulation will be discussed.

III.2 Overview of OFDM

OFDM is a particular form of Multi-carrier transmission and is suited for frequency selective channels. The main feature of this technique is the ability to transform a frequency selective wide-band channel into a group of non selective narrowband channels which makes it robust against large delay spreads. An other important feature of this modulation is the orthogonality in frequency domain. [28]. Furthermore the implementation cost of digital FFT modulators make OFDM particularly appropriate for frequency selective channels.

We previously derived the input/output relationship of a channel corrupted by fading. One of the main concerns in transmission schemes is to retrieve x (t) from (1.3) that for convenience is here repeated for a LTI channel including AWGN.

$$r(t) = \int_{-\infty}^{+\infty} q(r)x(t-\tau)d\tau + n(t) \qquad (3.1)$$

The process of extracting x (t) is called equalization and the difficulty is mostly due to the frequency selectivity of the channel [28].

Moreover, the complexity of an equalizer grows with the channel memory. Therefore the cost, in terms of complexity and power consumption, of such an equalizer could be prohibitively high, especially in the case of high data rates communications.

The main idea behind the OFDM transmissions is to convert the channel convolutional operation into a multiplicative one. This process will greatly simplify the equalization task. To realize this, a redundancy, known as **cyclic prefix CP**, is added in a smart way in order to circularize the channel effect. Due to the fact that circular convolution can be diagonalized on an FFT basis, the multipath time domain channel becomes a set of parallel frequency flat fading channels. Let us see how.

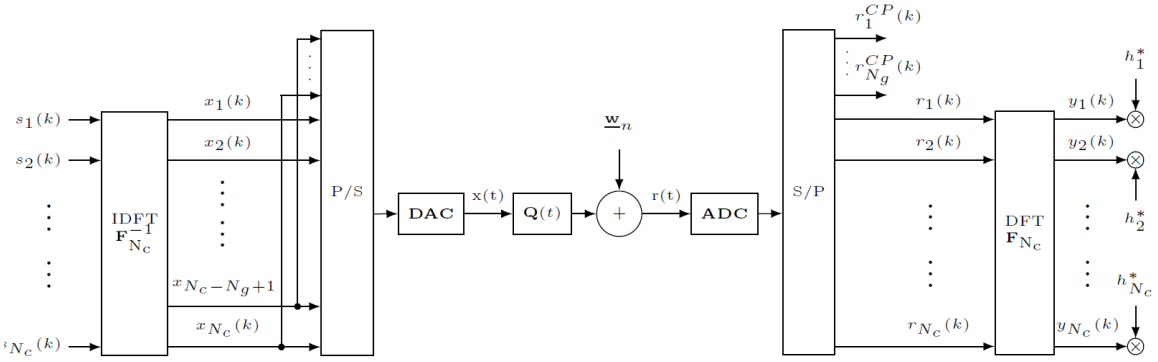

Figure 3.1: OFDM Block Diagram

The OFDM transmission block scheme is represented in Figure 3.1. As a starting point, we will consider the noiseless transmission case, finally the AWGN noise will be added to the model.

The high data rate is split onto N_c subcarriers. The data is thus, transmitted by blocks of size N_c : $s\,(k) = \left[s_1(k), \ldots, s_i(k), \ldots, s_{N_c}(k)\right]^T$, where the index k is referred to the kth block OFDM symbol and the subscript i to the i^{th} carrier. The block OFDM symbol is now precoded thanks to the use of the Inverse Discrete Fourier Transform (IDFT) to yield the so-called time domain block vector $(k) = \left[x_1\,(k), \ldots, x_i\,(k), \ldots, x_{N_c}(k)\right]^T$:

$$IDFT\{X[i]\} = x[n] = \frac{1}{\sqrt{N_c}} \sum_{i=0}^{N_c-1} X[i] e^{\frac{j2\pi ni}{N_c}}, 0 \le n \le Nc-1 \qquad (3.2)$$

$$DFT\{x[i]\} = X[i] = \frac{1}{\sqrt{N_c}} \sum_{n=0}^{N_c-1} x[n] e^{\frac{j2\pi ni}{N_c}}, 0 \le i \le Nc-1 \qquad (3.3)$$

The multiple orthogonal subcarrier signals, in fact, can be produced by IDFT defined in (3.2) and DFT defined (3.3) processes performed at the transmitter and receiver side respectively [7].

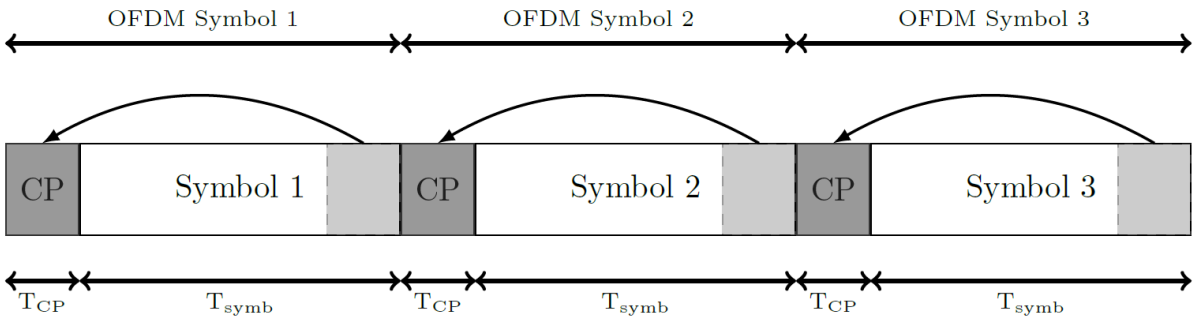

Figure 3.2: Time Domain OFDM symbols

Furthermore, DFT and IDFT can be efficiently implemented by using Fast Fourier Transform (FFT) and Inverse Fast Fourier Transform (IFFT). Note that it is possible to convert such expressions into a matrix form.
At the output of the IFFT (thus in the domain time), in order to mitigate the Inter- Symbol Interference (ISI) between OFDM symbols, a guard interval CP, composed by Ng samples, is inserted at the beginning of each block [28]. In Figure 3.2 this procedure is depicted. It consists of a cyclic extension of the OFDM symbol of size larger than the channel impulse response ($Ng > L - 1$). This redundancy, appended between each block, is able to transform the multipath linear convolution into a circular one.
In this context, it is important to remark that some constraints have to be satisfied and some tradeoffs have to be accepted. Due to problems related to the spectral inefficiency, in fact, the number of subcarriers Nc has to be much larger than the length of CP N_g.
However, the larger Nc, the greater the FFT complexity becomes.
Find a correct value of subcarriers, therefore, is a slightly tricky task because depends on the type of channel (slow varying, fast fading, channel length,...) and also on the complexity cost.
After the Parallel to Serial (P/S) and Digital to Analog Conversion (DAC) the signal is transmitted through a frequency selective channel.

The channel, as explained in, can be represented by a discrete time model and its effects can be modeled by a linear Finite Impulse Response (FIR) filtering with impulse response $q_{N_c} = [q_0, \dots, q_{L-1}, 0, \dots, 0]$.

Symmetrical operations will be performed at the receiver side to the received signal r(t) that, obviously, will still contain the CP. Then, after the Analog to Digital Conversion (ADC) and the Serial to Parallel (S/P) conversions, the cyclic prefix will be removed from the signal. This yields the discretized version of the signal $y\ (k)$ described in matrix form as in

$$\begin{bmatrix} y_1(k) \\ y_2(k) \\ \vdots \\ \vdots \\ y_{N_c}(k) \end{bmatrix}_{[N_c,1]} = F_{N_c} \begin{bmatrix} q_0 & 0 & \cdots & 0 & \ddots & q1 \\ \vdots & \ddots & \ddots & \ddots & \ddots & \vdots \\ q_{L-1} & \ddots & \ddots & \ddots & \ddots & q_{L-1} \\ 0 & \ddots & \ddots & \ddots & \ddots & \vdots \\ \vdots & \vdots & \ddots & \ddots & \ddots & 0 \\ 0 & \cdots & 0 & \cdots q_{L-1} & q_2 & q_0 \end{bmatrix}_{[N_c,N_c]} F_{N_c}^{-1} \begin{bmatrix} s_1(k) \\ s_2(k) \\ \vdots \\ \vdots \\ s_{N_c}(k) \end{bmatrix}_{[N_c,1]} \quad (3.4)$$

We may observe how, thanks to the use of the CP, we have converted the linear convolution into a circular one. Now, knowing from [29, 30, 31] that any circulant matrix in the Fourier basis is diagonal, we are able to easily diagonalize the channel through the use of Nc-point FFT [28].
At the output of such a multiplication we thus obtain the following expression:

$$\begin{bmatrix} y_1(k) \\ y_2(k) \\ \vdots \\ \vdots \\ y_{N_c}(k) \end{bmatrix}_{[N_c,1]} = \begin{bmatrix} h_0 & 0 & \cdots & 0 & \ddots & 0 \\ 0 & h_2 & \ddots & \ddots & \ddots & \vdots \\ \vdots & 0 & \ddots & \ddots & \ddots & 0 \\ 0 & \ddots & \ddots & h_i & \ddots & \vdots \\ \vdots & \vdots & \ddots & \ddots & \ddots & 0 \\ 0 & \cdots & 0 & \cdots 0 & 0 & h_{N_c} \end{bmatrix}_{[N_c,N_c]} \begin{bmatrix} s_1(k) \\ s_2(k) \\ \vdots \\ \vdots \\ s_{N_c}(k) \end{bmatrix}_{[N_c,1]}$$

(3.5)

where the signal $[s1\ (k), \dots, s_i\ (k), \dots, (k)]^T$ is transmitted over Nc parallel flat fading channels, subject each to a complex frequency attenuation hi. It is thus clear, that, starting from (3.5) we can easily equalize the channel through a multiplication of a bank of equalizers $h^* = (h_1^*, h_2^*, \dots, h_i^*, \dots, h_{N_c}^*)$.
The same approach can be applied in case of noisy transmission. The time Gaussian noise vector $w(k) = \left[w_1, \dots, w_i\ (k), \dots, w_{N_c}\ (k)\right]^T$ is multiplied by the FFT demodulator:

$$\begin{bmatrix} n_1(k) \\ n_2(k) \\ \vdots \\ \vdots \\ n_{N_c}(k) \end{bmatrix}_{[N_c,1]} = F_{N_c} \begin{bmatrix} w_1(k) \\ w_2(k) \\ \vdots \\ \vdots \\ w_{N_c}(k) \end{bmatrix}_{[N_c,1]} \quad (3.6)$$

Since the statistics of a Gaussian distribution do not change by orthogonal transform, the vector $n\ (k) = \left[w_1, \dots, w_i\ (k), \dots, w_{N_c}\ (k)\right]^T$ will be still Gaussian with the same covariance.

Figure 3.3 shows a representation of the frequency equivalent model of OFDM.

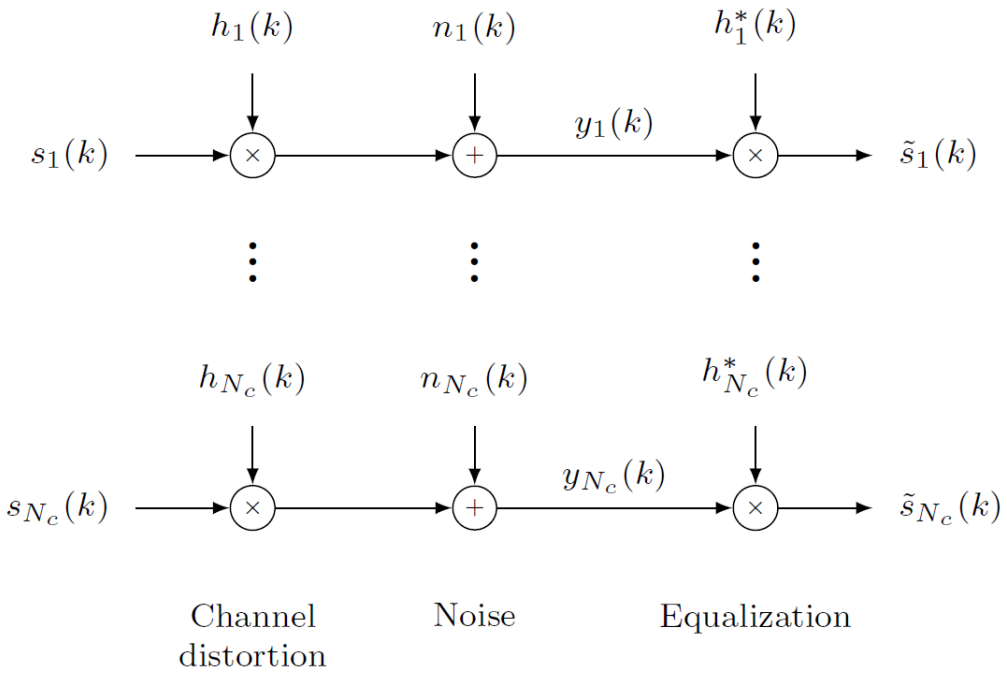

Figure 3.3: OFDM frequency domain model

III.3 OFDM Features

In the previous section, the operating principle of OFDM has been described. In this section, some considerations on the OFDM will be exposed.

III.3.1 Advantages

Immunity to selective fading: One of the main advantages of OFDM is that it is more robust to frequency selective fading than single carrier systems. We, in fact, showed how, thanks to the use of the cyclic prefix, OFDM is able to convert a frequency selective channel into the a collection of flat fading sub-channel [28].

- Spectrum efficiency: Subcarriers spectral efficiency is increased by allowing frequency overlapping of the different carriers. This yields an efficiency usage of the available bandwidth. Simpler equalization task: One of the issues with CDMA systems was the complexity of the channel equalization which had to be applied across the whole channel. In OFDM, the channel equalization becomes much simpler since the conversion in sub-channel [28]. Indeed, provided that the impulse response of the channel is shorter then the guard interval, each symbol is multiplied by the channel frequency coefficient and there is no Inter-Symbol Interference (ISI). The channel can be thus compensated for by a multiplication of each FFT output sample bya single coefficient. Among other schemes equalization schemes, zero forcing or Minimum Mean Square Error (MMSE) equalization (which takes into accountthe noise enhancement) is performed at the receiver.
- Interference robustness: During the transmission there may occur interference. In order to prevent such conditions, OFDM uses the guard interval named

cyclicprefix in multipath environment. This allows to keep amplitude and phase ofsubcarriers in orthogonal to the destination.

III.3.2 Drawbacks

Frequency off set vulnerability: OFDM is very sensitive for frequency off set as well as carrier synchronization problems. This problem can lead to Inter Carrier Interference (ICI) implying the destruction of the orthogonality between subcarriers or in a phase shift on the estimated symbols [28]. This sensitivity, which increases with the constellation size, is mostly affected by the N times longer duration of an OFDM block symbol and by the inter carrier interference due to loss of the carrier orthogonality.

High peak to average power ratio: An OFDM signal has a noise like amplitude variation and has a relatively high large dynamic range, or peak to average power ratio. This impacts the RF amplifier efficiency as the amplifiers need to be linear to accommodate for the large amplitude variations and these factors mean the amplifier cannot operate with a high efficiency level.

Chapitre IV
Multiple-Input Multiple-Output

Chapter IV

Multiple-Input Multiple-Output

IV.1 Introduction

The enthusiasm for wireless communications is undeniable. Phone operators are constantly looking for new services to offer to users, and multimedia applications are at the forefront of current business strategies. Supporting the telephony of real-time video transmission services (videophone) is at the study of many service providers. The challenge will therefore be to develop transmission systems that provide all of its applications in terms of throughput and robustness, MIMO systems have the potential to improve the performance of transmission without increasing the power or the bandwidth.

IV.2 Narrowband MIMO System

The MIMO technique consists of transmitting different blocks of information in parallel by using multiple antennas in transmission, that is to say at the input of the radio channel, and in reception, that is to say at the output of the radio channel . A MIMO system comprises of a number Mt of transmitting antennas and a number Mr of antennas in reception. Through the radio channel, each antenna receives the direct signal intended for it but also the indirect signals intended for the other antennas.

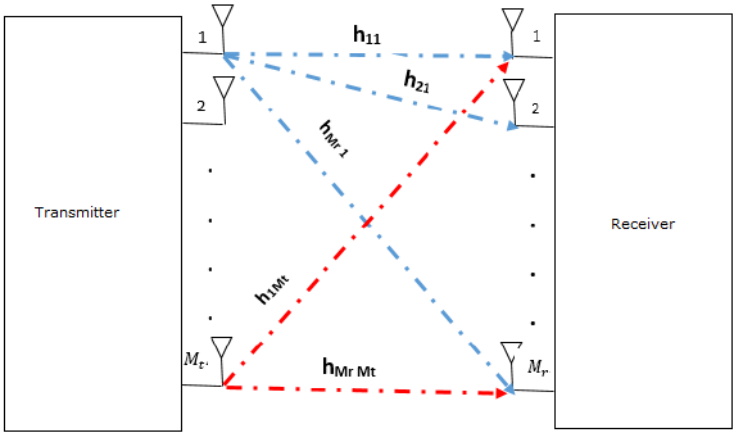

Figure 4.1 : MIMO system

This system can be represented by the discrete time model as follows:

$$r = Hs + n \tag{4.1}$$

Where:

r : represents the reception vector such that $r \in C^{M_r \times 1}$.

H : represents the matrix of the channel such as $H \in C^{M_r \times M_t}$.

s : represents the transmission vector such that $s \in C^{M_t \times 1}$.

n : represents the AWGN noise vector such that $n \in C^{M_r \times 1}$.

IV.3 Narrowband MIMO System

From the general model above, three cases exist[32]:

- SIMO: or receiver diversity, and consists of employing only one transmitting antenna and several receiving antennas, that is to say that the receiver receives the same signal by several antennas, these signals will then be combined, thereby reduces interference.

- MISO: or diversity in transmission, and consists in employing only one receiving antenna and several transmitting antennas. The diversity in transmission exploits multiple antennas at the transmitter level to introduce diversity, transmitting redundant versions of the same signal on several antennas. This type of MIMO technique uses what is called STBC and will be processed later.

- SISO: traditionally, when a single antenna is used in transmission and reception, the transmission technique on the radio interface is called SISO

IV.4 Signal detection for spatial multiplex MIMO systems

MIMO spatial multiplexing systems can transmit data at a higher speed than MIMO systems using antenna diversity techniques. However, detection of the signal is challenging. This section covers the three main detection techniques for MIMO multiplexing systems:

IV.4.1 Detector with Linear filtering

The linear detection of the signal consists in applying a linear filtering on the received signal. Two types of filtering are commonly used for spatial multiplex MIMO detection:

- Zero Forcing:
  The technique ZF cancels the interferences by applying to the received vector the matrix W_{ZF} called the pseudo-inverse of the matrix H and which is written in the following way:
  $$W_{ZF} = (H^H H)^{-1} H^H$$
- Minimum Mean Square Error:
  The detection MMSE consists in applying to the received vector the matrix W_{MMSE} which minimizes the mean square error at the sampling times between the symbols and the transmitted symbols. The matrix W_{MMSE} is defined by the following relation:
  $$W_{MMSE} = \left(H^H H + \sigma_n^2 I_{M_r}\right)^{-1} H^H$$

IV.4.2 Maximum Likelihood detector

The detector ML calculates the Euclidean distance between the received vector r and the product of all the possible transmission vectors with the matrix of the H channel and finds that distance. Mathematically this results in the following equation:

$$s_{ML}^* = argmin \left||r - Hs|\right|^2 \; s \in A^{M_t}$$

A : represents the constellation considered, of size M.

This type of detection is optimal in terms of error rates, but it has a complexity that increases exponentially with the size of the received vector and the modulation order.

IV.5 Receiving Diversity

In the case of diversity in reception, the variants of the transmitted signal whose fluctuations are decorrelated, will be combined, on reception, in such a way that the fading of the resulting signal is reduced. Most combination techniques are linear. The output of the combiner is only a weighted sum of the different receiver branches as shown in the figure below:

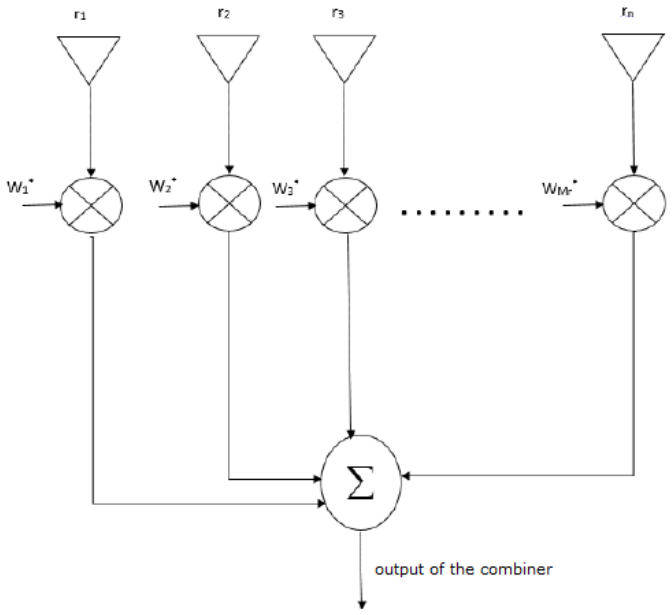

Figure 4.2: Linear combiner

IV.6 MIMO system for frequency selective channel

At the beginning of the chapter, we hypothesized that the MIMO system was narrow-band and therefore each transmitter-receiver link underwent a flat fading, but in fact the MIMO system is subject to a frequency selective fading due to the effect multi-paths of the channel. In this case the equalization of the channel is very complex and may require great computing power. To circumvent this problem and thus simplify the process of equalization of the channel, the MIMO system is associated with the multicarrier modulation [7] .

IV.7 Massive MIMO

Generally a communication system can be called massive MIMO when large number of antennas are employed at the BS side. However we do not have a precise definition since the number of transmitting antennas may vary according to the communication environment and the application [33]. We thus consider a system be massive MIMO when the BS is equipped with hundreds or thousands antennas.
In this section shall describe the massive MIMO system and investigate the theoretical advantages and drawbacks when such an approach is adopted [34].

IV.7.1 Advantages

Massive MIMO systems show several advantages mostly due to the capacity increasing without the usage of additional frequency spectrum. They present great robustness in the case of large attenuation due to path loss and a significant improvement in the spectral efficiency. Furthermore, the employment of a huge number of transmitting antennas allows us to have a better coverage area and guarantees to serve several users simultaneously.
Other consideration are discussed in the following subsections.

IV.7.2 Array Gain

Suppose a BS equipped with hundreds antennas placed within a cell serving multiple users, each one equipped with Nr receiving antennas. Usually modern devices such as smartphones have Nr = 2. The usage of massive MIMO has as first benefit the array gain. We know in fact that, under certain requirements, the SNR is proportional to the number of transmitting antennas Nt. Hence, by employing large number of antennas we can achieve a very large SNR [35].

Chapter V
Architecture of a SWIPT receiver

Chapter V

Architecture of a SWIPT receiver

V.1 Introduction

In this chapter, we propose an implementation for energy harvesting for a receiver with multi antennas. The signal received by the antennas first passes through a power splitter, where a part of the signal will be used for the information decoding and the remaining for energy harvesting. The aim is to define the hardware constraints for energy harvesting in a MIMO OFDM system.

V.2 The power splitter

In the Power splitting architecture as shown in Fig. 13, the received baseband signals are split into two streams, where one stream with power ratio $0 \leq r \leq 1$ is used for EH, and the other with power ratio (1 – r) is used for ID.

The design of the system is based on the power splitter for several reasons:

- More practical in implementation than the time splitter
- The power splitter archives better tradeoffs between information rate and the amount of energy transferred

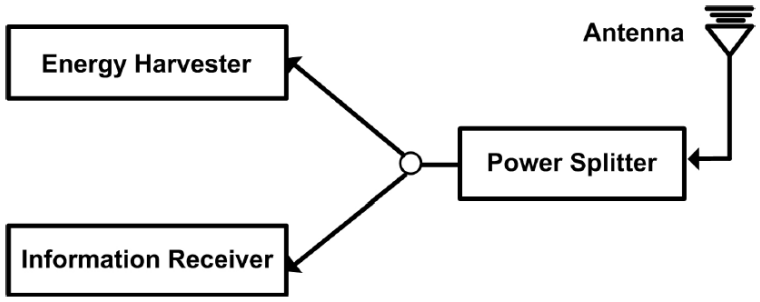

Figure 5.1: The power Splitter [1]

To simplify the implementation of energy harvesting at the receivers in the MIMO OFDM system a baseband model is used instead of the passband model which requires the implementation of the RF part at the transmitter and the receivers; and the hardware failure can be estimated and simulate.

This approach, which guarantees the fidelity of the model for the transmission of information from the transmitter to the receivers, is unfortunately not well adapted with the

Energy Harvesting system where the bandwidth of the circuit (diodes, capacitors) depends not only on the energy and the waveform of the received signal but also the static characteristics of the circuit and the frequency.

The solution proposed to solve this problem (to shift the frequency to the RF domain) and to keep the simplicity of the design is to apply an up mixing just after the splitter, an approach that is completely false for the decoding. But it can be used to analyses average EH at the passband thanks to Perceval's theorem.

$$\int_{-\infty}^{+\infty}|x(t)|^2dt = \int_{-\infty}^{+\infty}|X(f)|^2df \tag{5.1}$$

$$\int_{-\infty}^{+\infty}|x(t)\cos(2\pi f_c t)|^2dt = \frac{1}{4}\int_{-\infty}^{+\infty}|X(f+f_c)|^2df = \frac{1}{2}Ex \tag{5.2}$$

From Perceval's theorem, we notice that the average of the energy of the signal before the up mixing is twice the average of the energy of the signal after the up mixing, this factor of two can easily be implemented to reproduce the same average of the energy.

V.3 The matched Network design

After the Up mixing of the Energy harvesting signal coming from the power splitter, this signal supplies the rectifier circuit but before the rectifier circuit the design of the matching circuit related to the antenna impedance is very important to minimize the power reflected and increase the efficiency at the input of the rectifier circuit.
The energy harvesting circuit consists of diodes, which are non-linear devices, the circuit itself exhibits non-linearity. This implies that the impedance of the energy harvesting circuit varies with the frequency and the amount of energy received from the antenna, which make the design of the matched filter more challenging. For a first implementation the matched impedance is optimized for a determined distance from the base station. An essential factor for any RF application is proper impedance matching to the antenna, since without a passive LC network, much of the power received at the antenna will be reflected back into free space. The specifics of this matching process vary based on the antenna, and also upon the passive methodology of the receiving circuit input.

V.4 The rectifier circuit design

The rectifier circuit is characterized by the power conversion efficiency (PCE) or RF to DC conversion efficiency, is an important rectification metric for optimal wireless power transmission and is calculated as follow equation:

$$PCE = \frac{DC\ output\ power}{Incident\ RF\ Power - Reflected\ RF\ power} \tag{5.3}$$

The voltage multiplier structure is considered for RF-DC power conversion system design because it rectifies peak-to-peak voltage from the full-wave of the RF signal. Two configurations are arranged in a cascade using Schottky diodes to provide a passive voltage offset before rectification. The conventional voltage multiplier rectifier forms a peak rectified by D1 and C2, while a voltage clamp is formed by C1 and D2. The circuit can be also called a voltage doubler, thereby, the output voltage is approximately twice the input voltage. In the Villard topology the stages are connected in series and behave similarly to batteries in cascade, multiplying the output voltage. Fig 14 illustrates a two stages Villard voltage multiplier circuit, sometimes also called Cockcroft-Walton voltage multiplier, and Dickson voltage multiplier, Both Villard and Dickson topology reveal no significant difference in performance [36].

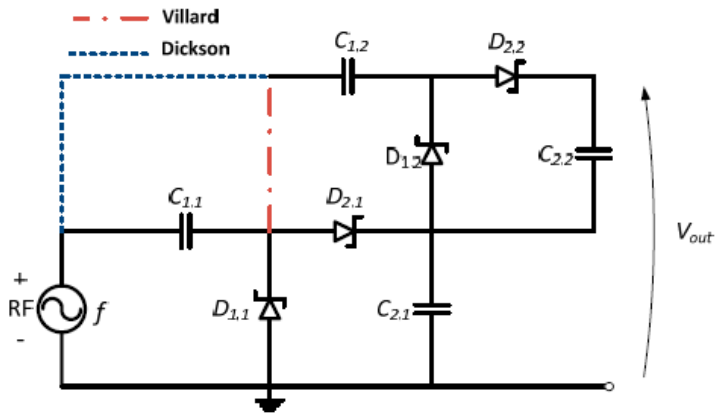

Figure 5.2: Two stage Villard and Dickson configuration for a combined voltage multiplier rectifier circuit

During an alternating voltage V is applied to the input of the circuit, the diode D1 will be blocked during all the negative half-cycle while the diode D2 will conduct and the capacitor C1will charge to the voltage Vmax. During the positive alternation. The diode D1 will conduct, charging the capacitor C2 at a voltage equal to twice Vmax due to the series connection of the voltage V and the voltage of the capacitor C1, By multiplying the number of the stages, it is possible to double the rectified voltage if the input voltage is sufficiently higher than the junction voltage of the diodes used. The doubling of the voltage at the output of the circuit passes through a transition period which is due to the charging time of the capacitors C1 and C2.

V.5 The Power management and the battery

The output of the rectifier represents the end of energy harvesting and the beginning of energy management. The circuitry placed at this terminal is responsible for maintaining a steady and continuous stream of power, preventing voltage spikes, power dropouts, excessive ripple, or any other unwanted characteristics that could disrupt performance. Some power management circuits may contain nothing but a voltage limiting Zener diode; others may contain complex arrays of active and passive elements that store power, emulate resistance, and dynamically regulate voltage. Depending on the application, whenever the harvested energy is more than that of the user's consumption, the excess energy will be stored in the battery for future use. The decision of what power circuitry to use is tied to the circuit application and the design-based tradeoffs [1].

Chapter VI
Simulation Analysis

Chapter VI

Simulation Analysis

VI.1 Introduction

This part of this thesis is dedicated to the development of the single user Single- Input Single-Output (SISO), Multiple Users - Multiple-Input Multiple-Output (MU-MIMO) simulators, and finally the circuit of the energy harvesting will be integrated on MIMO receivers. Such works have been entirely implemented using the MATLAB and Multisim softwares.
We shall proceed step by step starting with the SISO simulator that will give us the basic pillars in order to develop a higher complexity system, namely the MUMIMO/ massive MIMO simulator and then SWIPT receiver. At the end of the chapter, system performance, in terms of Bit Error Rate and efficiency of the harvesting circuit will be discussed. For this model, [27],[36] was used as guideline.

VI.2 SISO Transmitter

The SISO transmitter block diagram is depicted in Figure 6.1.

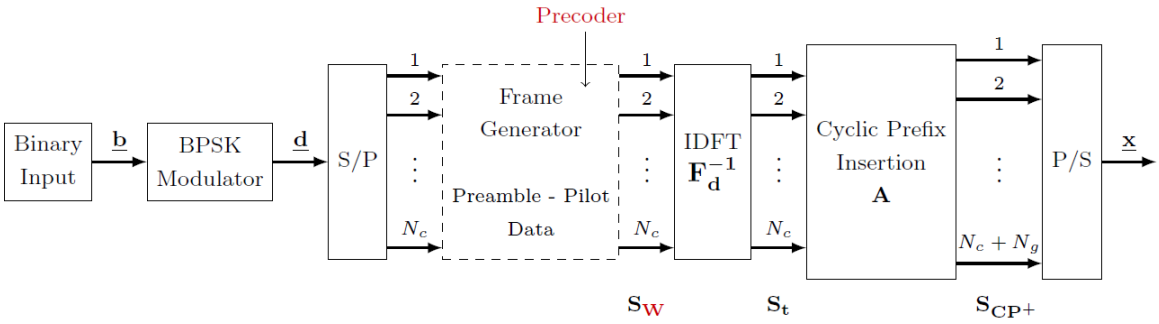

Figure 6.1: SISO OFDM Transmitter

- **Constellation Mapper**

An input bit vector $b \in [0\ 1]$of size K is mapped through Binary Phase Shift Keying (BPSK) modulation into the symbol vector b_d (of size K), whole elements belong to the alphabet $A = [-1, +1]$.Serial to parallel conversion is performed on the sequence $b_d$for frame generation in the frequency domain.
Depending on the number of subcarriers N_c, and on the number of symbols K, we may need to add dummy symbols in order to fill the remaining empty subcarriers.
We thus define the dummy symbol vector $b_d \in C$ of size $K_p = K_c - K$ where $K_c = N_c(1 + \left[\frac{K}{Nc}\right])$ and [.] denotes the floor function. These symbols are appended to d_d in order to obtain a new data vector $d = [d_{d,d_p}]$ of size $K_c = K + K_p$. We remark that the

dummy symbol insertion is exclusively performed for the correct filling of a proper data matrix, thus, they do not play a role on the detection process.
Let analyze how the frame that will be transmitted through a channel effected by AWGN and Rayleigh multipath fading is generated.

- **Frame Generation**

Based on the transmission protocol used, the frame structure may change and may require significant time to be developed. However in each frame we can easily recognize three main elements: a matrix with pseudo-random entries $G \epsilon C_{[N_c,R_g]}$ called preamble, a deterministic matrix $P \epsilon C_{[N_c,R_p]}$named pilot, and a matrix of data $D \epsilon N_{[N_c,R_d]}$where $R_d = K_c/Nc$
For this work the resulting frame is generated by concatenating such matrices, so that

$$S = [G, P, D]_{[Nc,Rs]} \tag{6.1}$$

where we defined $R_s = R_g + R_p + R_d$.

- **Preamble Matrix G**

The preamble matrix G is used for time and frequency synchronization purposes at the receiver side and is composed by alternating BPSK symbols and zeros. Assuming to have e.g. $R_g = 1$ and N_c is odd, we get $g = \left[g_1, 0,0, \dots ,0, g_{\left[\frac{N_c}{2}\right]}\right]^T_{[Nc,1]}$, where $[.]$ denotes the ceil function and the operator T stands for transpose. Such BPSK symbols are shared with the receiver in order to perform a precise time synchronization, moreover, for equalization purposes, the receiver could estimate the channel by evaluating the received stream when the preamble g is transmitted. The presence of many zeros in the vector g may decrease the quality of the estimation, but linear interpolation techniques can be adopted to cope with this problem.

- **Pilot Matrix P**

The pilot matrix P is employed for the estimation of the channel. This matrix is built starting from a deterministic vector $p \epsilon C_{[Nc,1]}$ composed by pseudo-random symbols such that $P = p.\, 1^T_{R_p}$. The choice of the parameter R_p is important because if on one hand a high value of R_p allows us to have a precise channel estimation, on the other hand it decreases the spectral efficiency of the transmitter. Thus, depending on the environment an adjustment of such parameter could be necessary.

- **Data Matrix D**

We previously generated the compatible row stream for the transmission over N c subcarriers, then the data matrix $D \epsilon N_{[N_c,R_d]}$ is simply obtained by the serial to parallel conversion of the

stream d.
The frame S is thus, the result of the concatenation of such matrices as expressed in (6.1) and it is ready to be fed to the IDFT block for the time domain conversion.

However, before this process, it may be appropriate to insert an additional zero padding $Z = 0_{[Nc,Rz]}$for SNR estimation purposes at the receiver, such that

$$S_z = [S, Z]_{[N_c,(R_s+R_z)]} \tag{6.2}$$

- **CSIT**

Suppose, now, to have perfect CSIT (Channel State Information at the Transmitter). We can, therefore, exploit this knowledge in order to perfectly diagonalize the Rayleigh fading channel. The input frame S_z can be thus precoded thanks to the use a precoder matrix W such that

$$S_w = WS_z \epsilon C_{[N_c,(R_s+R_z)]} \tag{6.3}$$

In our study, the precoder matrix W was selected according to two different approaches: Zero-Forcing (ZF) and Minimum Mean Square Error (MMSE).

- **Zero-Forcing (ZF)**

If the channel response is H then the input signal will be multiplied by the reciprocal of it. In our case the ZF precoder matrix W_{ZF}will be of the form of

$$W_{ZF} = H_c^+ (H_c H_c^+)^{-1} \tag{6.4}$$

where H_c is the baseband block diagonal channel matrix of dimension $[N_c, N_c]$and H the Toeplitz channel matrix of dimension$[(N_c + N_g), (N_c + N_g)]$ [37]. ZF allows us to remove the effect of the channel, in particular ISI, from the received signal.

This precoder is ideal when the channel is noiseless but has disadvantages when the channel introduces noise. In the latter case, in fact, ZF precoder, in the attempt to completely invert the channel, will amplify the noise greatly at frequencies f where the channel has a small magnitude [37].

For this reason the MMSE precoder is a more appropriate solution.

- **Minimum Mean Square Error (MMSE)**

MMSE precoder does not eliminate ISI completely but instead minimizes the total power of the noise and ISI components in the output. The precoder matrix is defined as

$$W_{MMSE} = H_c^+ \left(H_c H_c^+ + N_0 I_{N_c}\right)^{-1} \tag{6.5}$$

By a simple comparison between (6.4) and (14.5), we can see how, apart from the term $N_0 I_{N_c}$, the equations are the same. In fact, when the noise term is zero, the MMSE precoder reduces to ZF precoder.

Once the frame S_z has been precoded, the frame S_w (eq 4.3) passes through the IDFT block.

- **IDFT**

We define the symmetric complex DFT matrix F_d, of size $[N_c, N_g]$, as in chapter 3. The time domain representation of the full OFDM frame is obtained as:

$$S_t = F_d^{-1}.S_w \epsilon C_{[N_c,(R_s+R_z)]} \tag{6.6}$$

The frame, thus generated, is ready to be fed to the cyclic prefix block.

- **Cyclic Prefix Insertion**

Cyclic Prefix insertion can be performed by the insertion matrix A given by

$$A = \begin{bmatrix} 0_{[N_g,(N_c-N_g)]}, & I_{N_g} \\ & I_{N_c} \end{bmatrix} \tag{6.7}$$

We now multiply this matrix by the input frame $S_t$as

$$S_{CP+} = A\, S\, \epsilon C_{[(N_c+N_g),(R_s+R_z)]}. \tag{6.8}$$

Due to the redundancy of the cyclic prefix, the size of the resulting matrix is increased.

In particular the last N_g rows of the input matrix will be copied and appended to the beginning of the frame. We remark that in order to correctly diagonalize the channel the constraint $N_g > L - 1$ must be satisfied, where L is the number of the channel coefficients (namely, the channel length).

- **Parallel to Serial**

The matrix S_{CP+} is fed to the Parallel to Serial block such that a row vector x is the output. This data stream can be transmitted over a Rayleigh fading channel that also introduces AWGN. At the receiver side, the single user will thus receive $y(k) = \sum_{l=0}^{L} h(l)x(k-l) + n(k)$ where n represents the AWGN.

Next section will treat the implementation of the SISO OFDM Receiver.

VI.3 SISO Receiver

Figure 6.2 shows the block diagram of the SISO OFDM Receiver. The first operation to perform is the time-frequency synchronization.
We can therefore move to the description of the Serial to Parallel conversion.

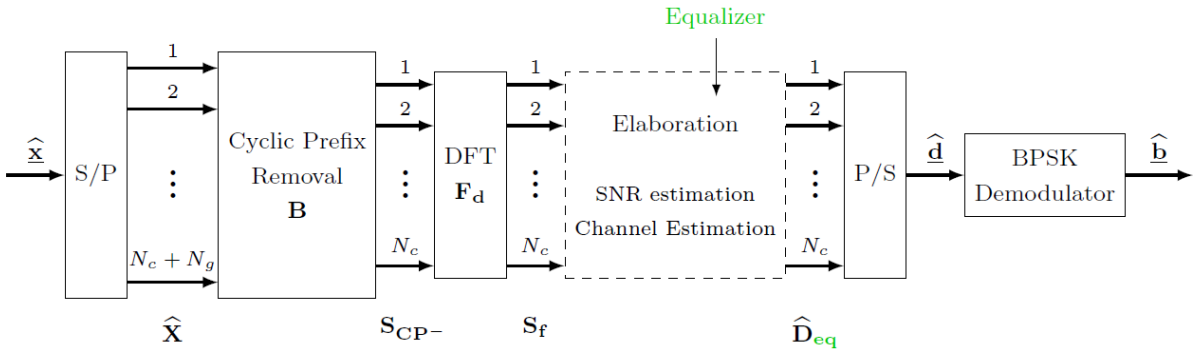

Figure6.2: SISO OFDM Receiver

- **Serial to Parallel**

The idea is to convert the data row vector y into a matrix of received data $\hat{X}_t$. This allows us to perform the cyclic prefix removal thanks the use of a matrix B as described below. The S/P conversion yields $\hat{X}_t = HC_{SP} + N\epsilon C_{[(N_c+N_g),(R_s+R_z)]}$ where we define N as the AWGN noise matrix in $C_{[(N_c+N_g),(R_s+R_z)]}$.

- **Cyclic Prefix Removal**

This operation is the dual operation w.r.t. the CP insertion at the transmitter side and is performed by the block B defined as

$$B = \left[0_{(N_c,N_g)},\quad I_{Nc}\right]_{[N_c,(N_g+R_z)]} \tag{6.9}$$

This block will delete the first N_g rows from the received stream $\hat{X}_t$so that the output is

$$S_{CP-} = B\hat{X}_t\, \epsilon C_{[N_c,(R_s+R_z)]} \tag{6.10}$$

At this point the matrix S_{CP-} is ready to feed the DFT block.

- **DFT**

The time samples are converted into frequency domain thanks to the use of the unitary DFT matrix $F_d$defined in Chapter 3. This reads

$$S_f = F_d S_{cp-} \tag{6.11}$$

S_f is thus composed by all elements of the received frame in the frequency domain, i.e., it is composed by the received pilot matrix $\widehat{P}$; , received preamble matrix $\widehat{G}$ and obviously by the received data matrix $\widehat{D}$.

We can simply identify this. frame as $S_f = \left[\widehat{G}, \widehat{P}, \widehat{D}, \widehat{Z}\right]_{C_{[N_c,(R_x+R_z)]}}$.

- **Processing**

The processing block performs the decoding procedure of the received signal. However, before this, receiver can exploit the structure of the transmitted frame in order to perform several operations such as the estimation of the SNR and the estimation of the channel. If CSIT is not available, in fact, we need to estimate the channel derive an equalizer.

We can thus compute an estimate of the SNR, denoted as $\widehat{\Gamma}$, the receiver defined as the ratio between the energy of the preamble G and the energy of the AWGN as expressed in the following equation

$$\widehat{\Gamma} = 10\, log_{10}\left(\frac{\hat{G}^{+}\hat{G}}{tr(\hat{Z}\hat{Z}^{+})}\right) \quad (6.12)$$

This formula is an approximation and it is strictly dependent on the size of the matrices. To obtain an accurate estimation, in fact, we need to have $R_z \gg 1$ and $R_g \gg 1$. Moreover it is more suitable for the high SNR regime. As previously mentioned, if CSIT is not available, the receiver can estimate the channel for equalization purposes.

The receiver evaluates the diagonal matrix $\widehat{H}_{eq} = diag\left(h_1^*, h_2^*, \dots, h_i^*, \dots, h_{N_c}^*\right) \epsilon C_{[N_c,N_c]}$ from the knowledge of the pilot matrix P defined in the previous section. Equalizer tap coefficients $\hat{h}_i$ are evaluated as

$$\hat{h}_i = \frac{1}{R_p}\sum_{j=1}^{R_p}\frac{\hat{P}_{i,j}}{P_{i,j}} \;\forall i = 1, \dots, N_c \quad (6.13)$$

We, then, simply invert the coefficients; and obtain $h_i^* = \frac{1}{\hat{h}_i} \forall i = 1, \dots, N_c$.

- **Parallel to Serial**

Equalized symbols, in the frequency domain, are converted from parallel to serial thanks to the use of P/S block. From this process we will thus obtain a row vector $\hat{d}_{eq} \epsilon C_{[1,(K+K_p)]}$that still contains dummy symbols. As previously mentioned, dummy symbols are not used for the detection procedure and for this reason, the last $K_p$elements will be removed from the stream. After this removal we obtain a vector $\hat{d}_{d,eq}$of size K which will feed the constellation demapper.

- **Constellation Demapper**

The input of BPSK demodulator is a row vector $\hat{d}_{d,eq} \epsilon N_{[1,K]}$ which is demapped into a vector $\hat{b}$ belonging to $[0,1]_{[1,K]}$.

- **Theoretical BPSK**

Knowing the channel gains, coherent detection of BPDK can be performed on a symbol by symbol basis, for a given value of channel gain, the error probability of detection is

$$Q\left(\sqrt{2|h|^2 SNR}\right)$$

Table 6.1: Characteristics of the simulated model

Modulation Format	BPSK
Number of subcarriers N_c	10
Channel length L	6
Cyclic Prefix Length N_g	7
Precoder type (only in the case of perfect CSIT)	ZF MMSE
Equalizer (only in the case of estimated channel)	ZF
SNR range	0-12dB

VI.4 Results

In this section we present the simulation results of the considered single user SISO OFDM system. The system performance is evaluated in terms of Bit Error Rate (BER).

At first we make a comparison between the two different approaches of Precoding in the case of perfect CSIT, namely ZF and MMSE, then subsequently we show the obtained results in the case of estimated channel with the presence of the equalizer at the receiver side. Furthermore results are compared with the theoretical BER curve of BPSK modulation over AWGN.

We take as reference a communication setup with characteristics described in Table 6.1. In particular we suppose to transmit 10^7 bits such that.

Figure 6.3 shows the obtained BER curves in the case of perfect CSIT using both Precoding algorithms. More precisely the red dotted line represents the theoretical BER curve for BPSK modulation in the case of AWGN channel, the circle markers black represent the obtained results in the case of Zero-Forcing Precoding, and obtained curve related to the MMSE Precoding the blue plus marks. We immediately realize how the three curves coincide.

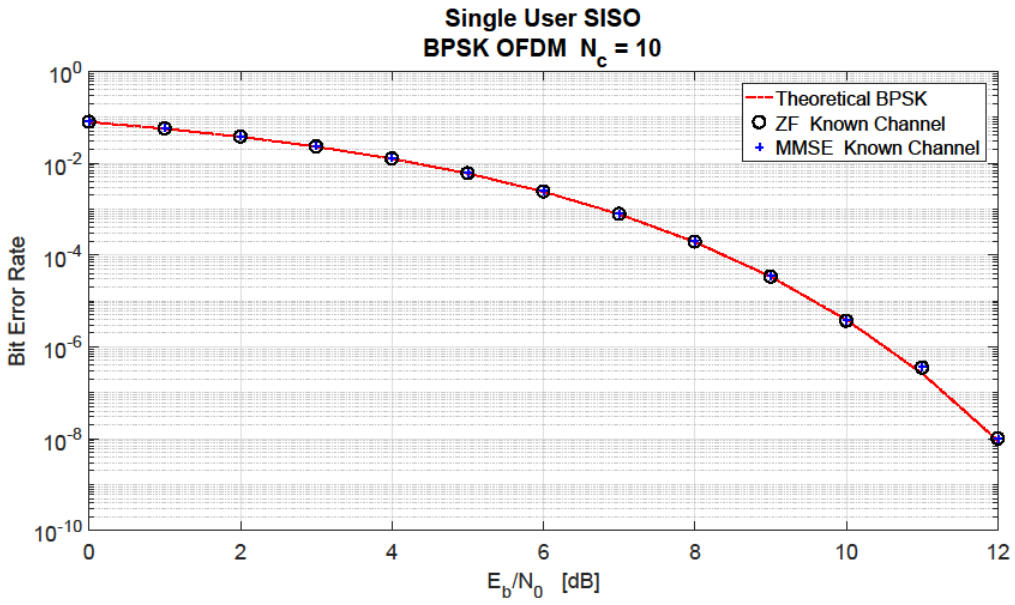

Figure 4.3: BER vs SNR plot. Comparison between Precoder algorithms

Supposing to have perfect CSIT, in fact, we are able to develop a perfect precoder which completely cancels the effects of the Rayleigh channel. In other words, thanks to the use of Precoding, the Rayleigh channel matrix is converted into an identity matrix on which the data are transmitted. The only noisy component that can affect the transmission therefore comes from the presence of Additive White Gaussian Noise (AWGN) on the channel. The behavior of such curves is then entirely analogous to the theoretical BER curve of a BPSK over AWGN channel. We note how at 11 dB there is a really small difference between the obtained curves and the theoretical case. However this difference is not significant for two main reasons: first, its entity is really minimal, second, it is not much reliable given that at 11 dB the BER value is below to 10^{-5}, our reliability threshold. Furthermore we remark how both precoding schemes yields equal performance.

Similar results are obtained in the case of channel estimation. In this scenario an equalizer is considered at the receiver side. Figures 6.4 and 6.5 depict a comparison between the theoretical BER curve, considered as before, and the simulated curve.

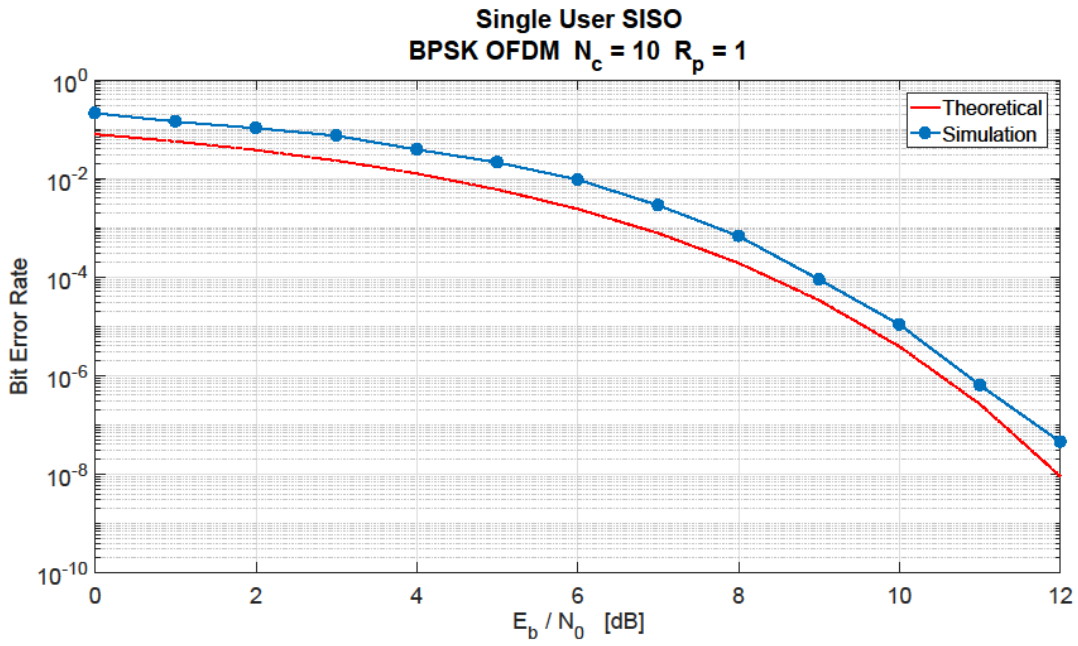

Figure 6.4: BER vs SNR with Equalizer. Rp = 1

By a simple comparison with the previous results we can observe how, in Figure 6.4, the obtained curve follows the same behavior of the theoretical one but it does not coincide exactly anymore. We note how, with the same BER, there is a loss of about 1 dB in the signal to noise ratio. This worsening is caused by two reasons. First, as previously mentioned the equalizer, may amplify the noise level. Such amplification will have the consequence of inducing the demodulator to an incorrect decoding, making more errors. Second, an unreliable channel estimation involves an inaccurate equalizer. In this case we are introducing another noisy component to the transmitted data since we are not able to perfectly cancel the effects of the Rayleigh fading channel.

If on the one hand, we can not avoid the amplification of the noise, on the other hand we can cope with such a problem by improving the channel estimation and therefore the equalizer procedure. We can in fact improve it by employing an higher number of pilot symbols, i.e. by increasing the number R p . This will give us a more precise equalizer as confirmed by Figure 6.5 where R p =10 . We note how the curve is qualitatively the same but the difference has been greatly reduced.

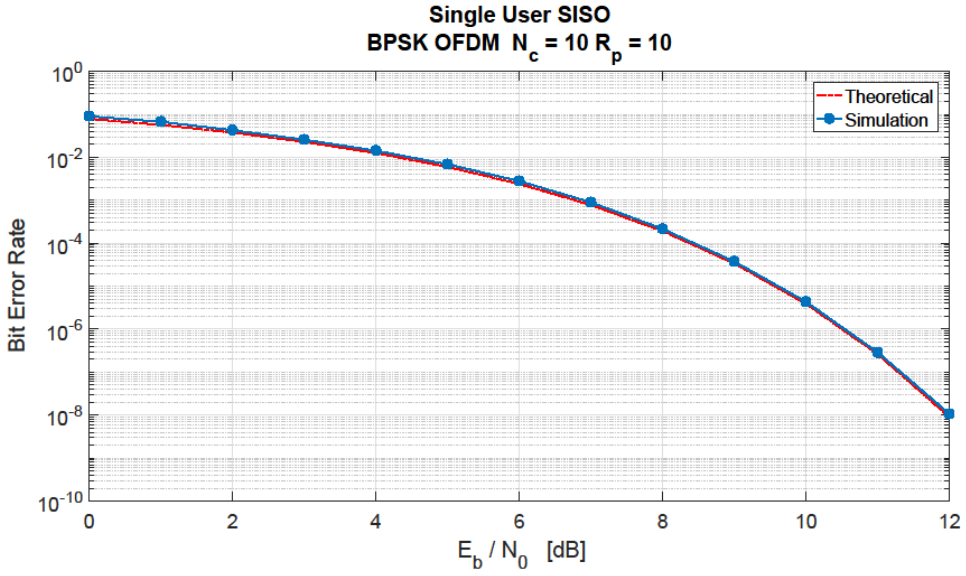

Figure 6.5 : BER vs SNR with Equalizer. Rp = 10

It is clear, then, by using an even higher number of pilots, the BER performance will coincide with the case of perfect CSIT shown in Figure 6.3.

VI.5 MIMO OFDM Simulator

In the previous Section we described a simulator for SISO communication based on OFDM for a single-user environment. In this chapter a suitable multi-user OFDM simulator is described. In particular, a parametric approach is adopted to yield a flexible tool able to simulate several LTE-like scenarios. For instance, the simulator could be used to model a standard MIMO communication (2 × 2 or 4 × 4) and a massive MIMO communication (16 × 2, up to a maximum limit, under certain conditions, of 1024 × 4).
The complexity but also the appromation the real scenario, compared to the SISO case, is increased. In this chapter, in fact, some novelties are presented such as the Scheduler function, the Equalizer function and the Users generation, while other components such as the Precoder function or the CP insertions/removal, will experience slight changes in order to be adapted for a communication system of this type. Furthermore three channel estimation methods (Ideal, RB and RBG) are considered.

We will proceed step by step with the implementation of this simulator.

VI.5.1 MIMO OFDM Transmitter

The MIMO OFDM Transmitter block diagram is shown inn Figure 6.7

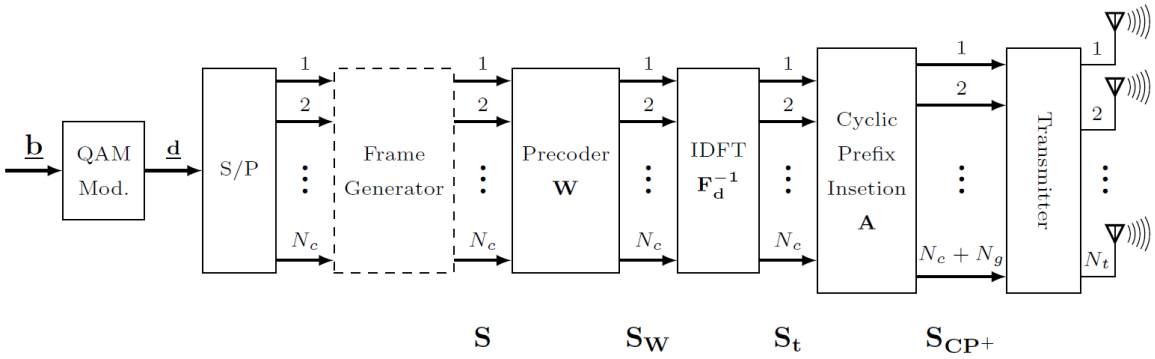

Figure 6.6 : MIMO OFDM Transmitter

- **Frame Generation**

This approach will be used as a guideline to design the corresponding frame structure suitable for a MIMO scenario.

Supposing to use a M-QAM modulation format and to transmit n bit , we can then define the minimum number of QAM symbols $K = \left[\frac{n_{bit}}{log_2 M}\right] = \left[\frac{n_{bit}}{k}\right]$, where k identifies the number of bits per symbol. Given that each user is equipped by N r receiving antennas, the current frame will be N_r times longer as compared to the SISO case. Under the condition of Normal CP, this yields a total of 140 $N_c N_r$ symbols per frame, denoted $N_{symb-frame}$. Even in this case we determine the total number of slots necessary to transmit K symbols as $n_{slot} = \left[\frac{K}{N_{symb\_frame}}\right]$.

We finally define the data matrix D belonging to C of size$[N_c N_r, n_{slot}]$. Such matrix can be divided into n_{slot} slots of size $[N_c N_r, 7]$and processed slot by slot avoiding memory problems as explained in the previous chapter.

- **Channel Estimation**

The channel estimation is performed before the transmission of the data. In fact, transmitter, sends to the receiver a pilot matrix P known to both sides. The receiver then, once processed it, feeds back quantized CSIT. The following Precoder is designed on the basis of such information. In this section we will present three different approaches to channel estimation.

Before entering the details of such estimation techniques, it is important to understand when the channel estimation is performed. We previously said, in fact, that the data matrix D is divided into blocks and processed slot by slot.

For this work, we perform an accurate estimation performed during the transmission of each slot which carries the data information. This means that we are assuming that channel does not change during the slot transmission. This is a reasonable hypothesis due to the fact that we are analyzing a femtocell environment and the transmission of one LTE slot lasts 0.5 ms.

It is possible to change this “channel step”, named τ_{tch}, following, in order to get a different channel scenario and a different estimation performance consequently. However, for this

work it has been set equal to the length in second of one LTE slot, i.e., $\tau_{tch} = 7(N_c + N_g)T_s$ where T_s represents the sampling time in ms.

Furthermore, the pilot matrix P is scaled by a factor α_p which takes into account the transmit power.

For all three estimation techniques we use the MMSE algorithm as explained in the following.

- **Ideal**

In this approach we suppose to be able to perform a perfect channel estimation. This means that the channel coefficients will be estimated for transmit and receive antennas in all subcarriers. It is clear that this is an idealized of estimation. In fact, even if from a computational point of view it is achievable, it is quite unthinkable that the receiver can deal with a feedback of such importance. However it is reasonable to consider this idealized case because it gives us a lower bound on the BER performance; we will expect, then, better performance when using this type of estimation.

An estimation of this type requires a Pilot matrix P defined as

$$P = \alpha_p \begin{bmatrix} p_{1,1} & \cdots & 0 \\ \vdots & \ddots & \vdots \\ 0 & \cdots & p_{N_c,N_t} \end{bmatrix}_{[Nc\ Nt, NcNt\ ]} \quad (6.14)$$

Pilot symbols $p_{i,j}$ are M-QAM symbols. In particular the subscript index i identifies the subcarrier while j identifies the transmit antenna. More precisely we say that $p_{1,1}$ is used to estimate the channel coefficient of the first transmit antenna in the first subcarrier, $p_{1,2}$ is used to estimate the channel coefficient of the second transmit antenna in the first subcarrier, while p_{1,N_t} is used to estimate the channel coefficient of the last N_t^{th} transmit antenna in the first subcarrier and so on.

We observe how the receive antennas are not specified. This is due to the fact that the baseband channel matrix, named H_c , is a block diagonal matrix of size $[N_cN_r, N_cN_t]$, as a consequence we may be able to estimate the channel gains of every receiving antenna in all subcarriers with a single pilot symbol. In particular, the generic pilot symbol $p_{i,j}$ is used to estimate the channel coefficient of the j^{th} transmitting antennas in the i^{th} subcarrier for the receiving antenna 1 up to N_r .

Every user will thus receive, from the BS, a matrix $H_{cp} = H_c\, P + noise$. By using an MMSE receiver, the channel can be estimated as

$$H_c = H_{cp}^{\dagger} \left(H_{cp}\, H_{cp}^{\dagger} + N_0\, I_{N_cN_t} \right)^{-1} \quad (6.15)$$

where the noise variance N_0 is used to regularize the inverse matrix since we normalize the average power per symbol to one. Once the estimation is complete, the receiver has to feed back this information to the BS, which will use it to set the Precoder.

At this stage, the redundancy which needs to be added in both downlink and uplink is rather clear. First, the transmitter needs to send entire OFDM symbols formed of just pilots, i.e., one pilot per resource element. Second, the receiver has to feed back $N_c\ N_t\ N_r\ = 12 n_{PRB}\ N_t\ N_r$ symbols to the transmitter in order to perfectly reconstruct the baseband channel model. It is evident how big this number can be even if a standard MIMO communication system is used in conjunction with the smallest number of subcarriers. For the LTE standard ($N_c\ = 71\ for\ B_x\ = 1.4\ MHz$), this number, where B_x represents the channel bandwidth, is quite big.

- **Resource Block**

A different approach is the RB estimation technique. The LTE frame is divided in PRB; we now wish to exploit this architecture in the estimation function.

A specific assumption can be made in this case. In particular, we assume that the frequency response of the channel in a PRB can be approximated by the channel gain at the subcarrier in that PRB. This will clearly diminish the redundancy for channel estimation at system level, at the cost of a reduction of the quality of the estimation as compared to the ideal case. In other words, remembering that a PRB is composed of 12 subcarriers, and supposing to have a 4 × 2 MIMO system, we may estimate the channel response between the 4 transmitting and 2 receiving antennas over the first subcarrier and extend the validity of the estimation to the whole PRB, i.e., 12 adjacent subcarriers. We remark that this is possible due to the fact the baseband channel, H_c , is a block diagonal matrix, thanks to the structure of the MIMO-OFDM transmission. An estimation of this type requires a pilot matrix expressed as

$$P = \alpha_p \begin{bmatrix} p_{1,1} & \cdots & 0 \\ \vdots & \ddots & \vdots \\ 0 & \cdots & p_{1,N_t} \\ p_{12N_t+1,1} & \cdots & 0 \\ \vdots & \ddots & \vdots \\ 0 & \cdots & p_{12N_t+1,N_t} \\ p_{k,1} & \cdots & 0 \\ \vdots & \ddots & \vdots \\ 0 & \cdots & p_{k,N_t} \end{bmatrix}_{[N_c N_t, N_t]} \tag{6.16}$$

We observe how the distance between each pilot symbols $p_{i,j}$, considering j fixed, is 12 N_t . In particular, the subscript k refers to the last PRB and it is therefore equal to $k = 12(\ n_{PRB}\ - 1\ )N_t\ + 1$, where n PRB is the overall number of PRB. Even in this case thanks to the channel model we can estimate all receiving antennas with a single pilot symbol.

Each user thus receives $H_{cp} = H_c P + noise$. Unlike before, we may apply the MMSE algorithm one PRB at a time in order to reduced the complexity of the matrix inversion step. Then, we obtain a matrix H i of size [$N_r \times N_t$] that will be inverted using the MMSE as

$$\widetilde{H}_c = H_i^{\dagger}\left(H_i H_i^{\dagger} + N_0 I_{Nr}\right)^{-1} \quad (6.17)$$

Note that the subscript index i of such matrix refers to the subcarriers, hence the rows $i = 12(m-1)\cdot N_r + 1 \; till \; 12(m-1)\cdot N_r + N_r$, $for \; m = 1,2,\ldots,n_{PRB}$.

Using this estimation method, receiver has to feed back to the BS a number of symbols equal to $n_{PRB} N_r N_t$ an overall saving therefore equal to 12 times with respect to the previous case.

- **Scheduler**

In general the scheduler is a component of an operating system that implements a scheduling algorithm which, given a set of requests for access to a resource, establishes a temporal order for the execution of these requests. A scheduler can privilege those requests that respect certain parameters according to a certain scheduling policy, so as to optimize access to this resource and thus allow the fulfillment of the desired service or process.

In this work, we consider a simplified schedule which is responsible of mapping users to sub-carriers for downlink transmission.

Ideally, we would want this process to yield fairness among users and minimize waste of resources (subcarriers). This choice therefore has strong impact on the performance, both in terms of bit error rate and average downlink throughput per user. There are several scheduling policies able to, for example, distribute subcarriers equally to users or able to maximize the performance associating a large number of subcarriers to users with the best channel conditions. There is therefore a continuous development and research of techniques and strategies in this area.

- **Precoder**

Precoding is a generalization of beamforming to support multi-stream (or multi-layer) transmission in multi-antenna wireless communications. In multi-user MIMO, a multi-antenna transmitter communicates simultaneously with multiple users (each having one or multiple antennas). This is known as space-division multiple access (SDMA). From an implementation perspective, precoding algorithms for SDMA systems can be sub-divided into linear and nonlinear precoding types. The capacity achieving algorithms are nonlinear, but linear precoding approaches usually achieve reasonable performance with much lower complexity. Linear precoding strategies include Maximum Ratio Transmission (MRT), Zero-Forcing (ZF) precoding, and Regularized Inverse (RI). There are also precoding strategies tailored for low-rate feedback of channel state information, for example random beamforming. Nonlinear precoding is designed based on the concept of DPC, which shows that any known interference at the transmitter can be subtracted without penalty on radio resources if the optimal precoding scheme can be applied on the transmit signal.

In this simulator, the precoder matrix W is defined from the knowledge given by the channel estimation. Precoder has the key role of spreading all the data information to each transmitting antennas and to form the beams suited for each user. Based on the scheduling

method adopted, in fact, the basestation inverts (or matches) the channel matrix in correspondence with the subcarrier to which a specific user has been associated.

The quality of this channel inversion depends on the channel estimation technique previously performed and on the mathematical approach adopted. We may expect, therefore, a more precise Precoder W in case of Ideal channel estimation and worse one in the case of RBG estimation.

At the end of this process the data frame D will be multiplied by the Precoder W such that the obtained frame $S_W = DW$ will be ready for the frequency time conversion. Furthermore three different approaches of precoding, namely ZF, MRT and RI, have been considered and compared.

- **Zero-Forcing Precoding**

Zero-Forcing (ZF) precoding is a method of spatial signal processing by which the multiple antenna transmitter can null multi-user interference signals in wireless communications.

If the transmitter knows the downlink CSI perfectly, ZF precoding can achieve almost the system capacity when the number of users is large. However if we have a limited CSIT the performance of ZF decreases depending on the accuracy of CSIT. Inaccurate CSIT, in fact, results in the significant throughput loss because of residual multi-user interference. Multi-user interference remains since they can not be nulled with beams generated by imperfect CSIT [38][35].

This solution has already been adopted in Section 6.1 in case of a SISO communication system. We will then explain only how this precoder is modeled in order to be suited for a MIMO system.
Remember that the baseband channel H c is a block diagonal matrix of size [$N_c\, N_r \times N_c\, N_t$] the resulting ZF precoding $W_{ZF} \epsilon\ C_{[\,(\,N_c\,N_r\,)\times(\,N_c\,N_t\,)]}$ will be of the form

$$W_{ZF} = \widetilde{H}_c^{\dagger}\left(\widetilde{H}_c\widetilde{H}_c^{\dagger}\right)^{-1}. \qquad (6.18)$$

We remark that the precoder is defined based on the channel estimation previously performed, hence the baseband channel is $\widetilde{H}_c$. Furthermore, we can efficiently implement this function one "block" at a time. More precisely, instead of performing the matrix inversion on the entire matrix $\widetilde{H}_c$ we can simply invert the desired subcarriers associated to the correct user [35].

- **Maximum Ratio Transmission Precoding**

A similar approach, based on concentrating on either the numerator or the denominator of the mentioned ratio is the Maximum Ratio Transmission (MRT) [35].

In order to maximize the SNR, the principle of Matched Filtering (MF), can be employed when CSI is available. In MIMO or massive MIMO context, we thus talk about MRT precoding. Such a scheme only maximizes the signal gain at the intended user. MRT is close-to-optimal in noise-limited systems, where the inter-user interference is negligible compared to the noise. In the limit of an infinite number of antennas serving a finite number of users, the effects of fast fading vanish and the channels of different users become orthogonal; thus MRT becomes optimal [35].

In math we can define MRT precoding a

$$W_{MRT} = \widetilde{H}_c^{\dagger}. \tag{6.19}$$

Note that even in this case we can efficiently perform this matrix inversion by "block" arrangement.

- **Regularized Inverse Precoding**

A trade-off between ZF and MRT is obtained by the so-called Regularized Zero-Forcing or simply Regularized Inverse (RI) Precoding. This approach, introduced by [39] , can be mathematically defined

$$W_{RI} = \widetilde{H}_c^{\dagger}\left(\widetilde{H}_c\widetilde{H}_c^{\dagger} + \beta I_{N_r}\right)^{-1} \tag{6.20}$$

Here β is the inverse of the transmit SNR per stream and is defined as $\frac{N_t N_0}{P}$ where P is the budget of total power [39]. By a simple comparison with (6.18) we can easily observe how the expressions are the same except for the regularization term βI_{N_r}. Furthermore RI can be implemented, by "block", as the previous one.

- **IDFT**

Frequency Time transformation is performed at the transmitter side thanks to the use of the IDFT algorithm. The precoded frame S W is converted in time through a multiplication with the symmetric IDFT matrix F_{Tx}

$$S_t \;=\; F_{Tx}\, S_W \tag{6.21}$$

with$S_t \epsilon C_{[(N_c N_t),n_{slot}]}$. The IDFT matrix F_{Tx} is defined as

$$F_{Tx} \;=\; F_d^{-1} \;\otimes\; I_{N_c} \,\epsilon\, C_{[\,(\,N_c \cdot N_t\,)\times(\,N_c \cdot N_t\,)]} \tag{6.22}$$

where varotimes denotes the Kronecker product, F_d^{-1} is the [$N_c \times N_c$] symmetric Fourier matrix as defined in previous chapters, and I_{N_c} represents the [$N_c \times N_c$] dimensional identity matrix [38].

- **Cyclic Prefix Insertion**

The redundancy interval addition, more precisely CP insertion, can be performed in matrix form as in explained in Chapter 3. However the insertion matrix A has to undergo slight changes with respect to the previous case.

CP insertion matrix is defined as

$$A = \begin{bmatrix} 0_{[(N_g N_t),(N_c - N_g)N_t]}, & I_{N_g N_t} \\ & I_{N_c N_t} \end{bmatrix}_{[(N_g + N_c)N_t, N_c N_t]} \tag{6.22}$$

We can observe how the dimension is expanded N_t times in order to be suitable for a N_t transmitting antennas [40].

Hence the time-domain frame S_t is multiplied by A such that

$S_{CP^+} \;=\; A\, S_t \,\epsilon\, C_{[\,(\,N_c + N_g\,)N_t \times n_{slot}\,]}$.

The frame, thus generated, can be transmitted through N t antennas by the basestation over the channel effected by Rayleigh fading and AWGN noise.

VI.5.2 MIMO OFDM Channel

In this section , the mathematical model used for the MIMO OFDM channel is detailed. The proposed channel scenario and the implementation of users are then described in this context. Finally, a section is devoted to all other channel parameters.

- **Mathematical modeling**

The received frame can be modeled in matrix form as

$$Y = H\,S_{CP^+} + N \quad \epsilon\, C_{[\,(N_c + N_g)N_t \times n_{slot}\,]}.$$

where the matrix H represents the Rayleigh channel, is block circulant with complex elements and has size $\left[\,\left(N_c + N_g\right)N_t \times n_{slot}\,\right]$ [40]. It is defined in (6.23) below and is composed by $h_j \sim CN\left(0, \frac{I_L}{L}\right)$ i.i.d. channel vectors of the L channel taps, representing the channel coefficient of the user [40]. The matrix N represents the AWGN matrix.

$$H = \begin{bmatrix} H_1 & 0 & \cdots & \cdots & 0 & H_L & \cdots & H_2 \\ H_2 & H_1 & 0 & \cdots & \cdots & 0 & \ddots & \vdots \\ \vdots & H_2 & \ddots & \ddots & \ddots & \ddots & \ddots & H_L \\ H_L & \vdots & \ddots & \ddots & \ddots & \ddots & \ddots & 0 \\ 0 & H_L & \ddots & \ddots & \ddots & 0 & \ddots & \vdots \\ \vdots & 0 & \ddots & \ddots & \ddots & H_1 & \ddots & \vdots \\ \vdots & \vdots & \vdots & \ddots & \ddots & \ddots & \ddots & 0 \\ 0 & 0 & \cdots & 0 & H_L & \cdots & H_2 & H_1 \end{bmatrix}_{[(N_c+N_g)N_r,(N_c+N_g)N_t]} \tag{6.23}$$

The general block matrix H_l (for l=1,2,...L) is a matrix of size [$N_r \times N_t$] which can be fully determined by its first column of size $\left[\left(N_c + N_g\right)N_r, \left(N_c + N_g\right)N_t\right]$. This "block matrix" is defined as

$$C = \begin{bmatrix} H_1 \\ H_2 \\ \vdots \\ H_L \\ 0[N_r\left(N_c + N_g - L\right), N_t] \end{bmatrix} \tag{6.23}$$

where 0 represents all zeros matrix having $[N_r\left(N_c + N_g - L\right), N_t]$ rows and N_t columns.

VI.5.3 MIMO OFDM Receiver

The block diagram of the MIMO OFDM receiver is shown in Figure 6.8.

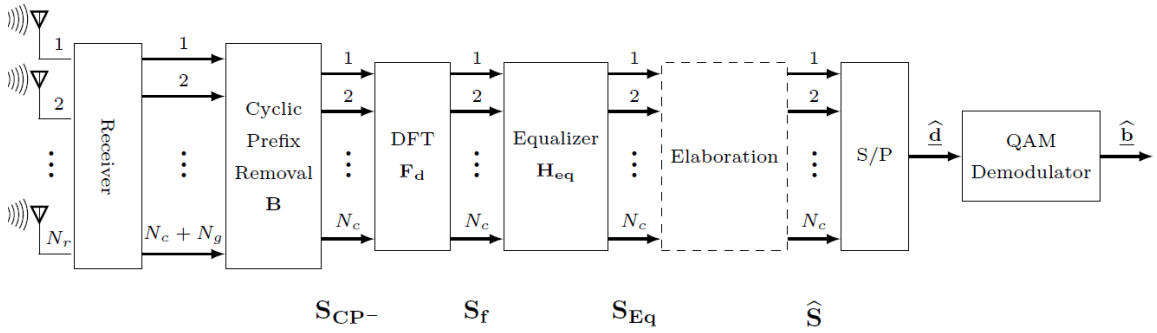

Figure 6.7: MIMO OFDM Receiver

- **Cyclic Prefix Removal**

First operation that has to be performed is the removal of the cyclic prefix. To this puropose, we can use as guide line the CP removal matrix adopted in the case of a SISO system in Section 6.1 [40]. Considering that each user is equipped with N r receiving antennas, the removal of this guard interval is ensured by the matrix B defined as

$$B = [\, 0_{[\, N_c N_r \times N_r N_g \,]}, I_{N_c} N_r] \tag{6.24}$$

By multiplying this matrix with the received frame$\hat{X}_t$; t of size $[\, (\, N_c + N_g \,) N_r \times n_{slot} \,]$ we obtain:

$$S_{CP-} = B\, \hat{X}_t \epsilon\, C_{[\, (\, N_c + N_g \,) N_r \times n_{slot} \,]} \tag{6.25}$$

- **DFT**

Once the cyclic prefix removal is complete, the received frame is ready to be fed to the DFT block. The dual transformation with respect to the transmitter side, in fact, is needed. Time frequency transformation can be performed in matrix form thanks to the use of the symmetric matrix F_{Rx} defined as

$$F_{Rx} = F_d \otimes I_{N_r} \epsilon\, C_{[\, (\, N_c N_r \,) \times (\, N_c N_r \,)]} \tag{6.26}$$

where F d identifies the symmetric Fourier matrix of size $[\, N_c \times N_c \,]$, $\otimes$ represents the Kronecker product and I N r is the identity matrix of size N_r [40].

The frequency domain output can be expressed as

$$S_f = F_{Rx}\, S_{CP-} \epsilon\, C\, [\, (\, N_c N_r \,) \times n_{slot} \,]\,. \tag{6.27}$$

- **Equalizer**

Equalizer is the other “new” function implemented for this model. Such a block has the main goal to cope with precoding errors performed at the transmitter side. Remember, in fact, that the precoder was developed based on the non-perfect channel estimation and thus could induce some errors that may cause a deterioration of the Bit Error Rate. We are, therefore,

motivated to combat such errors introducing an equalizer at the receiver side. To this end, an equalizer matrix $H_{Eq} \in C_{[\,(N_c N_r)\times(N_c N_r)]}$ has been designed. At the output of this block, we then obtained the equalized version of the received frame that can be expressed as

$$\widehat{D}_{Eq} = H_{Eq}\, S_f \in C_{[\,(N_c N_r)\times n_{slot}]} \tag{6.28}$$

however, it is appropriate to recall that, if on the one hand the equalizer can cope with precoder errors, on the other hand it may increase the noise power causing a significant performance reduction. Furthermore, we remark the equalizer adopted in this work is built upon the knowledge of the pilot symbol available at the receiver.

For this work two types of linear equalization algorithms have been adopted, namely Zero-Forcing (ZF) equalizer and Minimum Mean Square Error (MMSE) equalizer.

- **ZF Equalizer**

This linear equalization algorithm, used in many applications, was first proposed by Robert Lucky [41] and its name is due to the fact that it eliminates the ISI components to zero in the case of noiseless transmission.

It applies the inverse of the channel frequency response to the received signal in order to recover the signal after the channel. Hence, supposing that the BS has transmitted through the channel an M-QAM symbol p , each user receives the following:

$$H_B = Q_{Rx}\,(\,H Q_{Tx}\,\alpha_{Eq}\,p + noise\,) \tag{6.29}$$

where we collected in a compact form the baseband operation performed at the receiver $Q_{Rx} = F_{Rx}\,B$ and the baseband operations performed at the transmitter side $Q_{Tx} = A\,F_{Tx}\,W$. The scalar value α Eq is a normalization factor to satisfy the average power constraint and is defined as $\alpha_{Eq} = \frac{P_{Tx}}{N_t} \cdot$ P est where P_{Tx} is the transmitted average power by the BS and P_{est} represents the power of the transmitted frame after the baseband operations. In this way we ensure to have same the power for each transmitting antennas.

At this stage we can estimate this channel matrix by

$$H_{est} = H_B\, p^{\dagger}\,(\,p\, p^{\dagger}\,)^{-1}\,. \tag{6.30}$$

This matrix represents the estimated version of the block diagonal baseband channel matrix and can be processed by the ZF algorithm obtaining the equalizer

$$H_{Eq\,,ZF} = H_{est}^{\dagger}\left(\,H_{est}\;H_{est}^{\dagger}\,\right)^{-1} \tag{6.31}$$

We remark that this algorithm can be efficiently implemented “by block” following the same procedure adopted in the case of precoder matrix construction.

The main drawback of this equalizer, as stated previously, is the considerable noise power amplification. For this reason, a more balanced approach can be adopted.

- **MMSE Equalizer**

The Minimum Mean Square Error (MMSE) equalizer provides superior robustness to noise amplification by regularizing the matrix inverse using an appropriate factor. This estimator, is a well known method which minimizes the Mean Square Error (MSE) of the estimation/equalization, hence its quality.

As before, the frame received by each user is given by (6.29). For such reasons, we can implement the procedure in (6.30). Hence we can invert the channel frequency response by computing

$$H_{Eq,MMSE} = H_{est}^{\dagger} \left(H_{est} H_{est}^{\dagger} + N_0 I_{N_r} \right)^{-1} \quad (6.32)$$

where N_0 is the noise variance and I N r represents the identity matrix of size [$N_r \times N_r$] . We note that in the case of noiseless transmission the MMSE algorithm coincides with the ZF algorithm. Furthermore, it is possible to implement it “by blocks” similarly in the case of ZF previously stated.

- **Processing**

The processing block must decode the equalized version of the received noisy frame. To this end, first the equalized frequency-domain frame is converted, thanks to the use of a P/S converter, into a row vector.

At the output of this block we therefore obtain a row vector $\hat{\mathrm{d}}_{\mathrm{eq}} \in \mathrm{C}_{[\,1 \times \mathrm{N_c N_r n_{slot}}]}$ ready to be fed to the M-QAM demodulator. Subsequently the bit error rate is estimated.

VI.6 Results

In this section, the obtained results for the MIMO simulator are presented. We assess the system performance in terms of BER against the SNR. Our final goal is to estimate the penalty and then use the same system to study the energy harvesting, between the three proposed channel estimation algorithms, namely Ideal, RB and RBG.

In particular, since the channel estimation is performed thanks to quantized symbols that the receiver sends to the BS, we would like to find a trade-off between the penalty and the amount of data that has to be fed back to the transmitter.

We assume an indoor propagation scenario consisting a BS equipped with N t transmitting antennas placed within a cell serving multiple users N u , each one equipped with N r

Table 6.2: Simulator Setup 1

PARAMETER	VALUE
MIMO [N t × N r]	[32 × 2]
Channel Bandwidth	3 MHz
Modulation format	64-QAM
Scenario	EVA
PathLoss	ITU-R Commercial
Number of users N u	6
R min - R max	30 - 120 m
Speed (Doppler effect)	4 km/h
K RBG size (only in the case of RBG Estimation)	2 (standard)

receiving antennas. We remember that, for the sake of simplicity, we assumed that the number of users in the cell, is equal in each sector N u-sector . Thus, since the BS is divided into three equal sections of 120° each, the overall number of served users is Nu =3 Nu-sector. We suppose that users move within the cell with a velocity v km/h which takes into account the Doppler effect and, as previously stated, they are randomly displaced from the BS in a range R min - R max . For each user, we evaluate the BER values and the corresponding SNR range at the receiver side thanks to the processing block.

Furthermore, in order to have reliable results, the received signal is averaged over a number of iterations of noise realizations fixed at N iter =100 . The BS transmits with a power which goes from 20 or 23 till 32 dBm for indoor propagation, such that we will evaluate BER values around the 1 0 -2 ÷ 1 0 -4 with an SNR; Eb / N 0 where Eb is the energy per bit, of about 20 ÷ 30 dB. For the sake of compactness we report here the illustrative Table 6.2 regarding the simulator setups of the analyzed cases.

Figure 6.9 compares the three types of channel estimation methods for RI precoder and MMSE equalizer for Simulator Setup 1. As previously mentioned, the SNR can slightly change depending on the estimation algorithm proposed. We can observe how the curves representing the RB and RBG estimation coincide, while the curve representing Ideal estimation quickly drops.

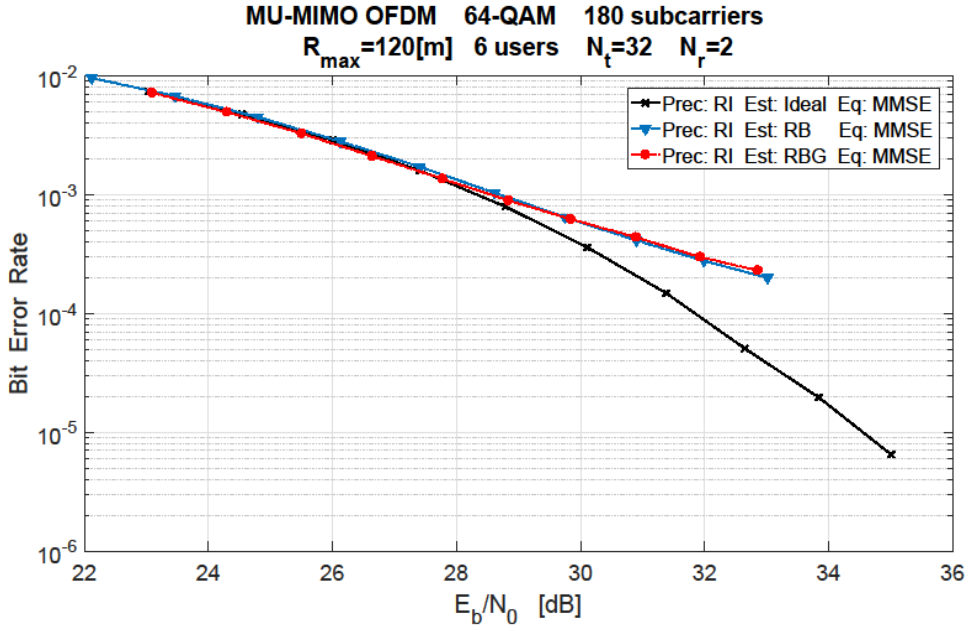

Figure 6.8: BER vs SNR. Simulator Setup 1

Comparison of channel estimation algorithms. Regularized Inverse Precoding (Tx side) - MMSE Equalizer (Rx side)

These results show how the Ideal channel estimation is a more precise algorithm with respect to the RB and RBG algorithms. Furthermore there is no benefit, in terms of error rate, on performing an RB estimation since it has equal performance than the RBG. In this case thus, by adopting an RBG we obtain a saving about 53.33% (or 448 symbols) on the feedback size without effects on the system performance. However, we note how, when operating in high SNR regime, the IE shows significantly better performance. For instance, by fixing E b / N 0 =32 dB we have that BER Ideal equals to 8.8 · 1 0 -5 and BE RRB equals to 2.7 · 1 0-4 .

Similar considerations can be drawn by the observation of Figure 6.10 .

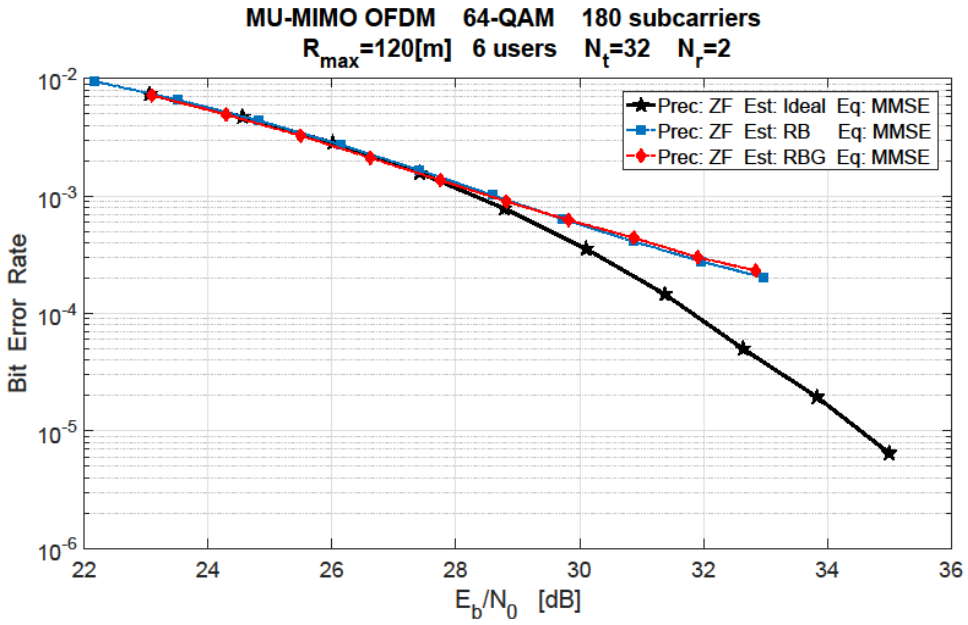

Figure 6.9 : BER vs SNR. Simulator Setup 1.

In this case, we employed a ZF precoding algorithm and, once again, an MMSE equalizer. Since the SNR range is the same, the comparison of the two cases is fair. We observe how the curves are basically the same, thus there is no impact, in terms of system performance, when using a RI or ZF precoder.

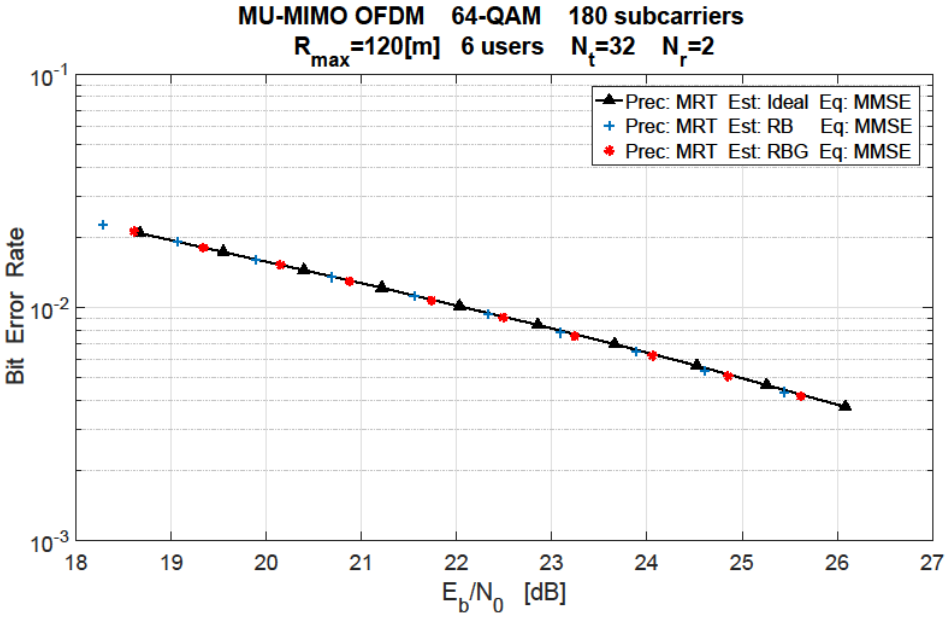

Figure 6.10 BER vs SNR. Simulator Setup 1.

Figure 6.11 shows the BER curves versus the SNR for an MRT precoder. The three curves coincide regardless the channel estimation techniques adopted. As a first look, it may seems theoretically wrong, however we have to take a look on the SNR range. In this case in fact, the use of the MRT precoder yields, as an effect, a rigid shift of the SNR range. In fact, if in the previous cases the SNR range was from 22 to 35 dB, here the range is displaced of 4 dB at least such that it goes from 18 dB to 26 dB. By observing this SNR range we can thus

compare the three precoding schemes just analyzed. Such results show how the curves coincide to each others. However, significant changes on the curves behavior are not shown. This is mostly due to the fact that MRT algorithm is only aimed at maximizing the signal gain at the intended user, thus, it may not to be sufficient in the case of communication in which the interuser interference is not negligible. Due to such issues, it is preferable to employ only the RI and ZF precoding algorithms because of their optimality.

VI.7 SWIP receiver

In this part the SWIPT system will be developer, one way to do, is to take advantage of the precarious part; of the MIMO OFDM system.

Therefore, the signal received by each user antenna will be converted to RF signal, the purpose of this part is to study the efficiency of the energy harvesting circuit in the same scenarios of wireless communication.

The antenna design is not taken into account in this thesis and the matching circuit between the rectifier circuit and the antenna will be automatically calculated by the Multisim tool.

VI.7.1 Rectifier circuit

As mentioned in [42], the rectifier topologies do not demonstrate a significant difference in performance. Hence, the Dickson topology (Figure 6.12), which has a parallel configuration of capacitors in each stage is chosen. The advantage here is that because of its the capacitors connected in parallel, the effective circuit impedance is reduced. Hence, this makes the task of matching the antenna side to the load side simpler.

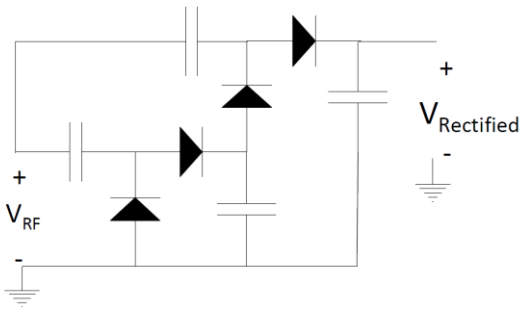

Figure 6.11 Dickson diode based multiplier

After choosing the Dickson topology, we next focus on the individual components that compose each stage and more precisely the diode, As it is developed in [43]. A packaged Schottky diode may be modeled as a nonlinear junction resistance Rj shunted by a non-linear junction capacitance C_j. V_j is the voltage loss at the rectifying junction. RS, LS and CP are the bulk resistance, packaging inductance and capacitance respectively [43]. A bare diode may also be modeled as a voltage controlled junction current source in parallel with a controlled capacitance (see Figure 6.12) and a parasitic bulk resistance [44]. IDC is the voltage controlled current source from the rectifying junction. Without neglecting the bulk resistance and the package parasitics, the controlled current source is treated as a DC source in parallel with a conductance G and a susceptance B. RD and XD are the parallel resistance and reactance of the diode respectively. IDC, RD and XD as in the linearized model are variables which depend on the diode parameters, input RF power PA, the connected DC load and the reflection coefficient at the input of the rectifier.

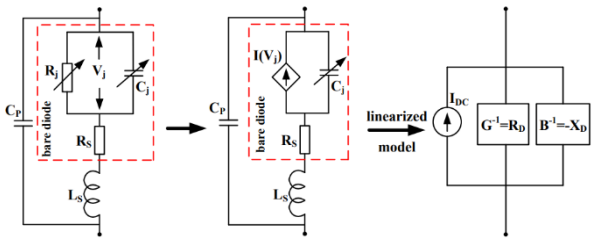

Figure 6.12 Schottky diode equivalent circuit models 45]

Parameter	Units	HSMS-285x
B_v	V	3.8
C_{J0}	pF	0.18
E_G	eV	0.69
I_{Bv}	A	3E-4
I_s	A	3E-6
N		1.06
R_s	Ω	25
$P_B(V_J)$	V	0.35
$P_T(XTI)$		2
M		0.5

Table 6.3 SPICE parameters

From Figure 6.13, the admittance of a Schottky diode may be written as in (3), where Y_{diode} is the diode admittance.

$$Y_{diode} = G + jB = \left(\frac{-jR_j\frac{1}{\omega C_j}}{R_j - \frac{1}{\omega C_j}} + R_s + j\omega L_s\right)^{-1} + j\omega c_p \qquad (6.33)$$

from the equation (6.33) and using the parasitic diode parameters in the table6.5 from the Schottky diode HSMS-285x series to calculate the diode impedance

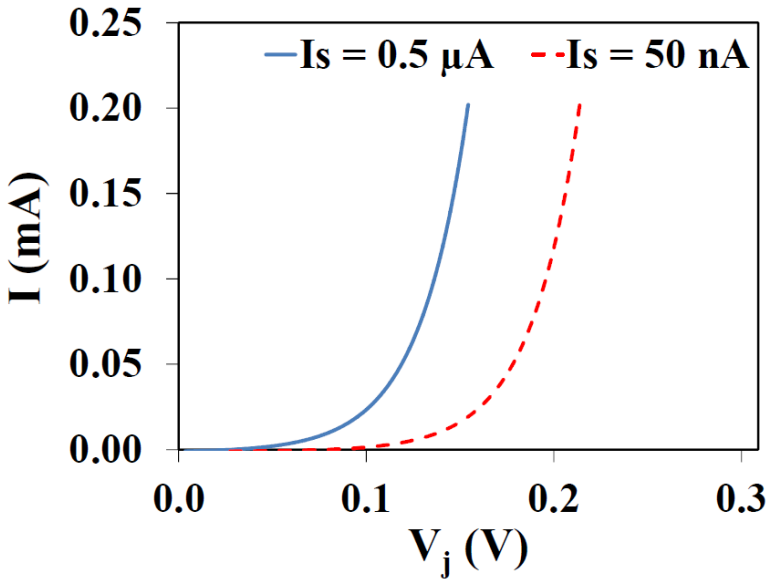

Figure 6.13: The effect of the changes in the equivalent circuit parameters of a Schottky diode[45]

Figure 6.14, shows that the efficiency of the schottky diode increase with high input voltage instead of high input current, therefore; To maximize Rd we need to choose the diode with

minimum current Is (saturation current), with minimum Cj (junction capacitances) and with minimum Rs (bulk resistances).

The characteristics lead us to choose the HSMS 1321 diode which satisfies all the constraints, widely available in the market and proven in several research papers by its efficiency[45].

Now, after choosing the topology and the diodes, The number of rectifier stages has a major influence on the output voltage of the energy harvesting circuit.

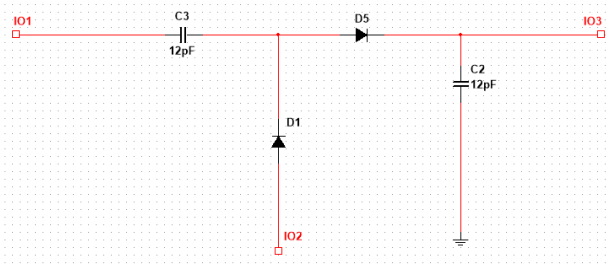

Figure 6.14 : Dickson Circuit

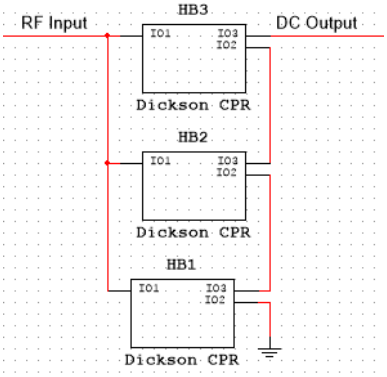

Figure 6.15 1Rectifier circuit with 3 stages

Figure 6.17 shows the impact of number of stages on efficiency. We have used Multisim with parameters sweep of −20 dBm to 20 dBm for the input RF power at 900 MHz and varies numbers of circuit stages from 1 to 4 stages.

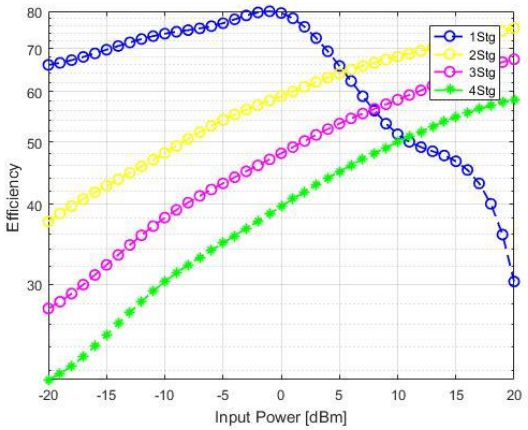

Figure 6.16: Effect of number of stages on the

We observe that the circuit yields higher efficiency as the number of stages increases with the input power. However, as more stages are introduced, the peak of the efficiency curve also shifts towards the higher power region, which leads us to a reasonable choice of one stage rectifier circuit for a simple reason is that the input power is less than 0 dBm by antenna in wireless communication system.

VI.7.1 SWIPT receiver simulation

In this part, the rectifier circuit with one stage developed in Section 6.4.1 will be integrated with soft power spliter into the MIMO OFDM system which is developed in 6.3 with the same parameters.

The following table summarizes the results of the simulation by user:

Table 6.4 SWIPT receiver results

Base station : 23dBm 32 antennas, 900Mhz. Users : 2 antennas					
Power Splitter mode	User	Distance (m)	Input Power (dbm)	BER (e-4)	Efficiency
20%	1	8	-47.19	4.6	23.3%
40%			-48.08	2.27	18.4%
60%			-50.28	1.6	16.6%
80%			-53.5	1.07	5.5%
20%	2	12	-51.0	5.0	12%
40%			-51.8	2.9	11.6%
60%			-53.34	2.0	3.4%
80%			-57.04	1.47	1.4%
20%	3	36	-60.0	8.12	<0.1%
40%			-61.5	4.83	<0.1%
60%			-63.7	3.46	<0.1%
80%			-67.0	2.33	<0.1%
20%	4	70	-66.31	18	<0.1%
40%			-68.26	13	<0.1%
60%			-69.65	11	<0.1%
80%			-72.34	9.25	<0.1%

We note that for systems that are within 12 meters are able to expect a BER of the order of e-4 and an efficiency between 23% and 1.4%, which motivates to develop splitters more adapted.
On the other hand for the users who are further from the base station, their efficiency is lower than 0.1% but they continue to reduce the BER with the input power.

Conclusion

Conclusion

In this Report, Simultaneous wireless information and power transfer simulator implemented with MATLAB and Multisim software have been presented.
The OFDM SU-SISO communication system gave us the fundamental basis from which develop a higher complexity system such as the precoded MU-MIMO/massive MIMO simulator.
In the Introduction of this thesis a brief but exhaustive state of the art on the wireless power communication is provided.

In Chapter 2 the main mathematical modeling and physical parameters of the wireless channel are discussed, making particular attention on the Rayleigh fading model.

In Chapter 3 we first treated the principle of OFDM suited for our purposes, then drawbacks and advantages of such modulation have been discussed.

The MIMO system was described in Chapter 4. In particular, we introduced the narrowband MIMO first, then an overview on the MU system and massive MIMO system has been provided.

In chapter 5 we propose an implementation for energy harvesting for a receiver with multi antennas. The signal received by the antennas first passes through a power splitter, where a part of the signal will be used for the information decoding and the remaining for energy harvesting. The aim is to define the hardware constraints for energy harvesting in a MIMO OFDM system.

In Chapter 6 we presented an OFDM Single User SISO simulator based on FDD for the downlink regime. System performance has been evaluated in terms of Bit Error Rate. We assumed an indoor propagation compromised by AWGN and Rayleigh fading noise. The data (BPSK modulated symbols) were split onto Nc subcarriers to employ an OFDM format. We supposed two scenarios: perfect CSIT and unknown channel. In the case of perfect CSIT two different precoder algorithms have been adopted, namely ZF and MMSE.

We proved the optimality of ZF precoding alogirthm and the MMSE equalizer when large pilot symbols are employed by comparing the simulated curves with the theoretical BPSK curve over a channel compromised by AWGN. We showed how the simulated and the theoretical curve coincide. Both algorithms, in fact, are able to perfectly diagonalize the channel such that AWGN is the only remaining drawback impacting the communication.
It has been shown that we need a significant number of pilot symbols (Rp = 10) in order to get analogous system performance to the case of perfect CSIT. However the higher the

number of pilot symbols, the lower the amount of data that can be transmitted. This condition can thus affect the spectral efficiency and power consumption.

Moreover, we remark that the presence of an equalizer may dramatically increase the noise level, inducing thus worse performance.
Then, MU-MIMO/massive MIMO simulator has been presented. System performance has been evaluated in terms of BER. Transmission in an indoor scenario compromised by AWGN and Rayleigh fading noise is considered. We assumed a BS equipped with Nt transmitting antennas, and serving multiple users Nu, each one equipped with Nr receiving antennas. We used 64/256 QAM modulation formats. Moreover, OFDM is employed such that the incoming data is split onto Nc subcarriers. A scheduler, at the transmitter side, allocates the resources (subcarriers) to specific users. Users were uniformly distributed from the BS within a range Rmin - Rmax m. Downlink communication occurred over the channel bandwidths fixed by the LTE standard.

Results showed that ZF and RI are optimal precoders and MMSE is the optimal equalizer. In scenarios in which large interuser interference occurs MRT is not a sufficient technique since it is only aimed at maximizing the signal gain at the intended user. After that, the rectifier circuit was designed based on the amount of the input power at the receiving antenna. The diode chooses is the HSMS and the number of stage is equal to one, the efficiency of this circuit is tested on Multisim, and it exceeds 50% for low input power.

The goal of the final simulation is the study of the efficiency and the Bit Error Rate in simultaneous wireless information and power transfer system. The result of the simulation shows that the SWIPT receiver have the ability to be integrated in the future low power consumption applications (IoTs) with a good BER / Efficiency ratio.

Future work

The developed simulator is a flexible and parametric tool which is able to simulate several and different LTE scenarios. Moreover, it is possible to set and change several parameters and algorithms. Hence, it can be considered a quite good solution to test wireless power communication system. However, we can improve the simulator.

We thus report here, the main drawbacks of the presented simulator that can be considered as future work.

- Increase flexibility
- Scheduling algorithm
- Coded transmission
- More Efficient Energy Harvesting circuit

REFERENCES

References

[1] X Lu, P Wang, D Niyato, DI Kim. "Wireless Networks with RF Energy Harvesting: A Contemporary Survey", IEEE Communications Surveys & Tutorials, Vol. 17, no. 2, pp. 757 – 789, November 2015.

[2] I Krikidis, S Timotheou, S Nikolaou. Simultaneous Wireless Information and Power Transfer in Modern Communication Systems, IEEE Communications Magazine, Vol. 52, no. 11, pp. 104 – 110, November 2014.

[3] A Van Zelst. MIMO OFDM for Wireless LANs, IEEE Transactions on Signal Processing, Vol. 52, no. 2, pp. 483 – 494, January 2004.

[4] X Zhou, R Zhang, CK Ho. Wireless Information and Power Transfer: Architecture Design and Rate-Energy Tradeoff, IEEE Transactions on Communications, Vol. 61, no. 11, pp. 4754 – 4767, November 2013.

[5] S Bi, CK Ho, R Zhang. Wireless powered communication: Opportunities and challenges, IEEE Communications Magazine, Vol. 53, no. 4, pp. 107 – 125, April 2015.

[6] "Wireless Power Transmission Market," Sep. 2015, Available on: https://www.marketsandmarkets.com/PressReleases/wireless-power-transmission.asp.

[7] Goldsmith Andrea. Wireless Communications, chapter 2. stanford university press,stanford,2005.

[8] MOHAMAD ELKHALED. Evaluation de la capacite du canal uwb minier. Master's thesis, Universite de Quebec en Abitibi-Temiscamingue, 2011.

[9] TESSERAULT Guillaume. Modelisation multi-frequences du canal de propagation. PhD thesis, Universite de Poitiers, 2006.

[10] Mohamed Maalej. Etude et implÃc mentation d'un systeme sans fil multi-antennes dans un contexte mc-cdma. Master's thesis, Ecole Polytechnique de Tunisie, 2008.

[11] Sylvie Picol. Conception et realisation de la partie numerique d'un simulateur materiel pourles canaux de propagation MIMO. PhD thesis, Institut National des Sciences Appliquees de Rennes, 2007.

[12] CHARTOIS YANNICK. Etude parametrique avancee de canaux SISO et MIMO en environnements complexes :Application au systeme HiperLAN/2. PhD thesis, ECOLE NATIONALE SUPERIEURE DES TELECOMMUNICATIONS DE BRETAGNE, 2005.

[13] Benoit Le Saux. Estimation de canal pour systemes multi-antennes multi-porteuses.PhD thesis, INSA de Rennes, 2007.

[14] Jean-Noel GOUYET and Sylvie KALINWSKI. Radio numerique -modulation ofdm. Techniques de l'ingenieur, page 22, Aout 2013.
[15] CHARTOIS YANNICK. Etude parametrique avancee de canaux SISO et MIMO en environnements complexes :Application au systeme HiperLAN/2. PhD thesis, ECOLE NATIONALE SUPERIEURE DES TELECOMMUNICATIONS DE BRETAGNE, 2005.
[16] MOHAMAD ELKHALED. Evaluation de la capacite du canal uwb minier. Master's thesis, Universite de Quebec en Abitibi-Temiscamingue, 2011.
[17] Edgard Haddad. APPORT DE LA MODELISATION DETERMINISTE 3D INDOOR POUR L'INGENIERIE DES SYSTEMES RADIO AVANCES. PhD thesis, l'Universite europeenne de Bretagne, 2011.
[18] Jean-Noel GOUYET and Sylvie KALINWSKI. Radio numerique -modulation ofdm. Techniques de l'ingenieur, page 22, Aout 2013.
[19] Sylvie Picol. Conception et realisation de la partie numerique d'un simulateur materiel pour les canaux de propagation MIMO. PhD thesis, Institut National des Sciences Appliquees de Rennes, 2007.
[20] CHARTOIS YANNICK. Etude parametrique avancee de canaux SISO et MIMO en environnements complexes :Application au systeme HiperLAN/2. PhD thesis, ECOLE NATIONALE SUPERIEURE DES TELECOMMUNICATIONS DE BRETAGNE, 2005.
[21] S. S. Ghassemzadeh, L. J. Greenstein, A. Kavcic, T. Sveinsson and V. Tarokh, "Indoor path loss model for residential and commercial buildings," Proc. Vehic. Technol. Conf., pp. 3115–3119, October 2003.
[22]
[23] V. Erceg, L. J. Greenstein, S. Y. Tjandra, S. R. Parkoff, A. Gupta, B. Kulic, A. A. Julius and R. Bianchi, "An empirically based path loss model for wireless channels in suburban environments," IEEE Selected Areas in Communications, pp. 1205–1211, July 1999.
[24] Goldsmith Andrea. Wireless Communications, chapter 7. stanford university press, stanford,2005.
[25] Serge DRABOWITCH. Antenne a traitement du signal. Techniques de l'ingenieur, page 22,Aout 2006.
[26] S. Weinstein and P. Ebert, "Data transmission by frequency-division multiplexing using the discrete fourier transform," IEEE Trans Comm Tech, pp. 628–634, 1971.
[27] R. Chang, "Synthesis of band-limited orthogonal signals for multi-channel data transmission," Bell System Technical Journal, pp. 1775–1796, 1996.
[28] M. Debbah, "Short Introduction to OFDM," CentraleSupélec - LANEAS Group - White Paper, 2004.
[29] G. H. Golub and C. F. Van Loan, Matrix Computations. John Hopkins University Press, 1996.
[30] R. A. Horn and C. R. Johnson, Matrix Analysis. Cambridge University Press, 1990.
[31] C. S. Burrus and T. W. Parks, DFT/FFT and Convolution Algorithms. John Wiley, New York, 1985.

[32] Jerome Pons. Reseaux cellulaires-evolution du systeme umts vers hcpa. Techniques de l'ingenieur, page 21, Mai 2011.
[33] E. G. Larsson, D. Danev, M. Olofsson and S. Sorman, "Teaching the Principles of Massive MIMO," Whitepaper, Oct. 2016, Available on: https://pdfs.semanticscholar.org/7298/e267b8b5d4f8ea122c97-ea97fbfa8039c210.pdf - Access date: 7/04/2017.
[34] D. Schoolar, "Massive MIMO comes of age. New active antenna technologies play a major role in the evolution of mobile broadband networks," Samsung, Tech. Rep., 2017, Available on: http://www.samsung.com/global/businessimages/insights/2017/Massive-MIMO-Comes-of-Age-0.pdf - Access date: 24/01/2018.
[35] T. L. Marzetta, E. G. Larsson, H. Yang, H. Q. Ngo, Fundamentals of Massive MIMO. Cambridge University Press, 2016.
[36] Chaour, Issam, Ahmed Fakhfakh and Olfa Kanoun. "Enhanced Passive RF-DC Converter Circuit Efficiency for Low RF Energy Harvesting." *Sensors* (2017).
[37] M. Maso, "Flexible cognitive small-cells for next generation two-tiered networks," CentraleSupélec - Whitepaper, 2013.
[38] Allert van Zelst, Tim C. W. Schenk, "Implementation of a MIMO OFDM-based wireless LAN system," IEEE Trans Signal Processing, vol. 52, no. 2, pp. 483–494, February 2004.
[39] C. B. Peel, B. M. Hochwald, A. L. Swindlehurst, "A vector-perturbation technique for near-capacity multiantenna multiuser communication-part I: channel inversion and regularization," IEEE Transactiom on Communications, vol. 53, no. 1, January 2005.
[40] M. Maso, M. Debbah, L. Vangelista, "A distributed approach to interference alignment in OFDM-based two-tiered networks," IEEE Trans Signal Processing, pp. 1935 – 1949, February 2013.
[41] R. D. Gitlin J., F. Hayes S., B. Weinstein, Data Communications Principles. Springer, 1992.
[42] H. Yan, J.G. Macias Montero, A. Akhnoukh, L.C.N. de Vreede, J.N. Burghart, "An Integration Scheme for RF Power Harvesting", The 8th Annual Workshop on Semi- conductor Advances for Future Electronics and Sensors, Veldhoven, Netherlands, 2005.
[43] T Beckedahl, T Ostertag, L Reindl," Analysis of Passive RF-DC Power Rectification and Harvesting Wireless RF Energy for Micro-watt Sensors", AIMS Energ, April 2015.
[44] Maas, Stephen A. Nonlinear microwave circuits, Boston ; London : Artech House, 2003.
[45] A Nimo, T Beckedahl, T Ostertag, L Reindl, Analysis of Passive RF-DC Power Rectification and Harvesting Wireless RF Energy for Micro-watt Sensors, AIMS Journal, 2015

[37] M. Maso, "Flexible cognitive small-cells for next generation two-tiered networks," CentraleSupélec - Whitepaper, 2013.

[38] Allert van Zelst, Tim C. W. Schenk, “Implementation of a MIMO OFDM-based wireless LAN system,” IEEE Trans Signal Processing, vol. 52, no. 2, pp. 483–494, February 2004.

[39] C. B. Peel, B. M. Hochwald, A. L. Swindlehurst, “A vector-perturbation technique for near-capacity multiantenna multiuser communication-part I: channel inversion and regularization,” IEEE Transactiom on Communications, vol. 53, no. 1, January 2005.

[40] M. Maso, M. Debbah, L. Vangelista, “A distributed approach to interference alignment in OFDM-based two-tiered networks,” IEEE Trans Signal Processing, pp. 1935 – 1949, February 2013.

[41] R. D. Gitlin J., F. Hayes S., B. Weinstein, Data Communications Principles. Springer, 1992.

[42] H. Yan, J.G. Macias Montero, A. Akhnoukh, L.C.N. de Vreede, J.N. Burghart, ”An Integration Scheme for RF Power Harvesting”, The 8th Annual Workshop on Semi- conductor Advances for Future Electronics and Sensors, Veldhoven, Netherlands, 2005.

[43] A Nimo,T Beckedahl, T Ostertag, L Reindl, "Analysis of Passive RF-DC Power Rectification and Harvesting Wireless RF Energy for Micro-watt Sensors", AIMS Energy, 2015.

[44] Maas, Stephen A. Nonlinear microwave circuits, Boston ; London : Artech House, 2003.

[45] A Nimo, T Beckedahl, T Ostertag, L Reindl, Analysis of Passive RF-DC Power Rectification and Harvesting Wireless RF Energy for Micro-watt Sensors, AIMS Journal, pp. 184-200, April 2015.